




## Interplay between biochemical processes and network properties generates neuronal up and down states at the tripartite synapse

Shubhada N. Joshi <sup>1,\*,\dagger</sup> Aditya N. Joshi <sup>2,\*,\ddagger,\S</sup> and Narendra D. Joshi <sup>3,\*,\|</sup>

<sup>1</sup>National Center for Adaptive Neurotechnologies (NCAN), David Axelrod Institute, Wadsworth Center, New York State Department of Health, 120 New Scotland Ave., Albany, New York 12208, USA

<sup>2</sup>Stanford University School of Medicine, 300 Pasteur Dr., Stanford, California 94305, USA

<sup>3</sup>General Electric Global Research, 1 Research Circle, Niskayuna, New York 12309, USA



(Received 10 April 2022; accepted 3 January 2023; published 21 February 2023)

Neuronal up and down states have long been known to exist both *in vitro* and *in vivo*. A variety of functions and mechanisms have been proposed for their generation, but there has not been a clear connection between the functions and mechanisms. We explore the potential contribution of cellular-level biochemistry to the network-level mechanisms thought to underlie the generation of up and down states. We develop a neurochemical model of a single tripartite synapse, assumed to be within a network of similar tripartite synapses, to investigate possible function-mechanism links for the appearance of up and down states. We characterize the behavior of our model in different regions of parameter space and show that resource limitation at the tripartite synapse affects its ability to faithfully transmit input signals, leading to extinction—down states. Recovery of resources allows for “reignition” into up states. The tripartite synapse exhibits distinctive “regimes” of operation depending on whether ATP, neurotransmitter (glutamate), both, or neither, is limiting. Our model qualitatively matches the behavior of six disparate experimental systems, including both *in vitro* and *in vivo* models, without changing any model parameters except those related to the experimental conditions. We also explore the effects of varying different critical parameters within the model. Here we show that availability of energy, represented by ATP, and glutamate for neurotransmission at the cellular level are intimately related, and are capable of promoting state transitions at the network level as ignition and extinction phenomena. Our model is complementary to existing models of neuronal up and down states in that it focuses on cellular-level dynamics while still retaining essential network-level processes. Our model predicts the existence of a “final common pathway” of behavior at the tripartite synapse arising from scarcity of resources and may explain use dependence in the phenomenon of “local sleep.” Ultimately, sleeplike behavior may be a fundamental property of networks of tripartite synapses.

DOI: [10.1103/PhysRevE.107.024415](https://doi.org/10.1103/PhysRevE.107.024415)

### I. INTRODUCTION

#### A. What are up and down states?

Up states, consisting of tonic neuronal firing with relatively depolarized resting membrane potentials, and down states, consisting of neuronal quiescence with relatively hyperpolarized membrane potentials, have long been described in both *in vitro* cortical preparations and *in vivo*, in both anesthetized

and behaving animals [1–3]. A variety of functions have been suggested for these oscillations, including synaptic plasticity, memory consolidation, cellular maintenance activities, and recovery of “fatigue variables” due to prolonged fast neuronal firing, and it may be that several or all of these functions occur simultaneously [1,4,5]. The mechanism for the transitions between up and down states is not clearly known, but it is generally accepted that the oscillations are due to the network properties of collections of neurons. These network effects appear to be primarily mediated by glutamatergic and GABAergic (GABA is gamma-aminobutyric acid) neurotransmission since the transitions are significantly diminished by glutamate receptor antagonists, and abolished by glutamate and GABA receptor antagonists, although there is evidence that other neurotransmitters such as dopamine may also play a role [6,7].

#### B. Existing models of up and down states

Computational models of the up and down phenomenon often rely on networks with recurrent excitation, and transitions between states are either driven by slow negative feedback processes such as firing rate adaptation or short-term synaptic depression, or are due to stochastic external noise in

\* All authors contributed equally to this work.

<sup>\dagger</sup>Present address: National Center for Adaptive Neurotechnologies (NCAN), Stratton VA Medical Center, Research 151, 113 Holland Ave., Albany, New York 12208, USA.

<sup>\ddagger</sup>Corresponding author: [adityanarjoshi775@gmail.com](mailto:adityanarjoshi775@gmail.com)

<sup>\S</sup>Present address: University of Pennsylvania Perelman School of Medicine, Department of Neurology, 3 West Gates Bldg, 3400 Spruce St., Philadelphia, Pennsylvania 19104, USA.

<sup>\|</sup>Retired.

Published by the American Physical Society under the terms of the [Creative Commons Attribution 4.0 International](https://creativecommons.org/licenses/by/4.0/) license. Further distribution of this work must maintain attribution to the author(s) and the published article’s title, journal citation, and DOI.

neuronal populations [1,6,8,9]. Most computational studies take one of two approaches to studying up and down states: (1) models with networks of integrate-and-fire neurons based on an electrical formalism to more closely replicate observed phenomena, and (2) population-level models that simulate large scale dynamics while abstracting individual neuronal-level processes, for example, [1,6,8–11]. Other models of the tripartite synapse will also briefly be reviewed.

### 1. Integrate-and-fire neuron network models for up and down states

The first class of models includes those which are based on networks of integrate-and-fire neurons. These are all phenomenological models: the modeled neuron generates a spike when its membrane potential passes a predetermined value. Membrane potentials are calculated based on solving systems of differential equations involving conductances and currents affecting each model neuron [12,13]. The integrate-and-fire neurons are then linked into networks with weights representing neuronal connectivity. These networks require some mechanism to drive the transitions between up and down states, and the mechanisms differ by specific model. Some of the mechanisms utilized to generate transitions between states include a nonlinear membrane current, an adaptation current, firing rate adaptation (including spike frequency adaptation), short-term depression, and network connectivity combined with noise [8,9,14,15]. There are various models which have attempted to utilize more “realistic,” physiologically based model neurons (such as [16–18]). The key features these models share are the inclusion of Hodgkin-Huxley dynamics (see [19,20]) instead of simple integrate-and-fire kinetics and the presence of multiple layers of connected neurons.

There was a single study, by Ching *et al.*, which attempted to more directly connect metabolic considerations to the Hodgkin-Huxley formalism by introducing an ATP (adenosine triphosphate) -gated current mediated by the  $K_{ATP}$  channel, and including the ATP-active  $Na^+/K^+$  ATPase pump. These authors modeled a network of “reciprocally coupled interneurons and pyramidal cells” [21] and found that the model was able to generate a pattern of bursts of activity with intervening periods of quiescence at the level of local field potentials, suggestive of neuronal up and down states. They likened these fluctuations to cortical “burst suppression,” which may be seen on EEG during general anesthesia.

Integrate-and-fire network models, and their Hodgkin-Huxley-based counterparts, are successfully able to generate states resembling neuronal up and down states, and have several advantages, including that they are capable of representing relatively complicated network connectivity effects, while still being relatively computationally tractable. They may include named or known synaptic currents, including excitatory AMPA ( $\alpha$ -amino-3-hydroxy-5-methyl-4-isoxazolepropionic acid) and NMDA (N-methyl-D-aspartic acid) receptor-mediated glutamatergic currents, and inhibitory GABA currents, or may simply consider the sum total of all synaptic currents without assigning them to specific channels. However, these models do not include any of the underlying biochemistry for the electrical effects they model. They thus cannot shed any light on why state transitions occur at any

specific time, nor what the function of the up and down states may be. They are also unable to explain how the same network can produce bistable state dynamics, and “stable asynchronous irregular dynamics” [8]. The single study which includes a connection to energy metabolism simply adds the  $K_{ATP}$  channel and sodium-potassium pump as additional currents, and modulates the ATP availability as an independent variable [21]. It is able to generate high and low levels of simulated activity based on energy scarcity, but still does not yield a mechanism for why the energy supply would be depleted in the first place, nor how the alteration of active and quiescent periods may ameliorate the low-energy state.

### 2. Mean-field models for up and down states

It has been noted that there are approximately  $10^{1.5 \times 10^{10}}$  possible configurations of neurons with binary (either activated or quiescent) states in the human brain. Because of the massive scale of calculating such configurations, and also because of the presence of “randomness” in both the connectivity and the neural activity in neuronal networks, such systems can be well approximated using statistical methods [10]. Models derived from these methods achieve dimensionality reduction by abstracting the dynamics of individual neurons, and making statistical assumptions about the behavior of entire neuronal populations, and are thus more computationally tractable. Such models are called *mean-field* models, and the Wilson-Cowan model and its extensions are the best-known members of this class [11,22]. The original Wilson-Cowan model was based on population dynamics of neurons using continuous time, and as such, inputs were considered to be [mean] spike frequencies, rather than individual spikes [11]. Later treatments have extended the mean-field method in various ways [10,22–25]. Other mean field models also exist, such as that found in Holcman and Tsodyks, which includes a population of excitatory neurons and a “depression parameter” [6].

The primary advantages of mean-field models are their significantly decreased computational burden—the original Wilson-Cowan model had only two differential equations—and their ability to capture large-scale behavior, even to the level of whole-brain networks [11,22]. In addition they can model “balanced” networks—a special case wherein random fluctuations can cause an irregular firing rate, rather than just creating two stable states [25]. However, mean-field models suffer from the same limitations as the integrate-and-fire network models described above. In fact, they have even less explanatory power at the neuronal level, since single-neuron-level dynamics are subsumed in the statistical treatment of the neuronal population. These models cannot explain, for instance, Li, Poo, and Dan’s important findings that stimulating *single* neurons through a patch clamp technique could switch the entire local network from an up and down bistable mode to a low amplitude, high frequency mode they named “persistent-up,” and vice versa, or similar findings by Fujisawa, Matsuki, and Ikegaya [26,27]. However, there was a study which examined how single-neuron properties distributed over the mean field could affect the firing of the whole network [28].

### 3. Electrical and diffusion-based models of the tripartite synapse

Many studies have looked at models of the tripartite synapse, and have been classified based on the primary focus of the model: those focusing on voltage-gated calcium channels, potassium dynamics, gliotransmission, learning, and electrical descriptions [29]. A large group of models treats with the ionic interactions between neurons and astrocytes, including calcium currents and potassium dynamics. Several of these models are based on a combination of the Hodgkin-Huxley formalism with the similarly formulated Li-Rinzel model for astrocytic calcium dynamics [29–32]. Other models investigate the impact of astrocytes on neuronal firing based on diffusion of small molecules—glutamate and “gliotransmitters” [29]. Models of astrocytic uptake of glutamate were based on diffusion, and did not include representations of ionic processes (for instance, see [33,34]). Models treating with gliotransmission did investigate ionic currents, particularly including calcium currents, and again used a combination of the Hodgkin-Huxley formalism and Li-Rinzel model, including [35,36], as did a model investigating the astrocytic contribution to learning [37]. The models with electrical descriptions were also based on the Li-Rinzel model [29].

These models of the tripartite synapse successfully model neuron-astrocyte interactions. They may include named or known synaptic currents, including excitatory AMPA and NMDA currents and inhibitory GABA currents, or may simply consider the sum total of all synaptic currents without assigning them to specific channels. However, the above-described models also do not include any of the underlying biochemistry for the electrical effects they model. Because of this, and that they do not specifically address neuronal up and down states, they are also unable to make any connection between a function and a mechanism of up and down states.

### 4. Neurochemical models of the tripartite synapse

There are only a few studies that investigate models which include the biochemical reactions taking place in different parts of the tripartite synapse, which we term “neurochemical models.” Jolivet *et al.* proposed a biophysical model including a neuronal compartment, astrocytic compartment, extracellular compartment, and a vascular compartment [38]. They extended prior work and generated a set of 33 differential equations, with compartmentalization between cytosolic and mitochondrial compartments in the neuron and the astrocyte, the inclusion of a Hodgkin-Huxley-type electrical model of synaptic firing, the provision of explicit glutamatergic input, and explicit calculation of sodium transport. Kinetics related to Michaelis-Menten kinetics was utilized to represent some enzyme-driven processes. Using this model, they were able to reproduce the evoked responses of various parameters seen in rat and human *in vivo* experiments. Patel *et al.* examined the relationship between glutamatergic neurotransmission and neuronal glucose oxidation in a seizure model using  $^{13}\text{C}$  nuclear magnetic resonance (NMR) [39]. As part of their study, they established a metabolic model to calculate  $^{13}\text{C}$  fluxes in the neuron and astrocyte, based partly on Michaelis-Menten kinetics. They found that neuronal activity, neurotransmitter cycling, and glucose oxidation were linearly

coupled over much of the range of neuronal activity. Several models investigate the metabolic fluxes between neurons (both glutamatergic and GABAergic) and astrocytes, but do not appear to (at least explicitly) include vesicular loading of neurotransmitter, nor synaptic release and reuptake, nor neurotransmission at all. Notably, they are also steady-state models, which cannot be readily applied to dynamically firing neurons [40–43]. We are not aware of any other models other than that by Jolivet *et al.* which try to connect the neurotransmission of neurons with their metabolic processes [38].

The model by Jolivet *et al.* does accommodate both neurotransmission and metabolic processes, and impressively, is able to match empirical measurements of metabolic processes *in vivo*, including in humans [38]. However, it utilizes Michaelis-Menten kinetics, which assumes at least a quasi-steady state, and may not be realistic for dynamically firing neurons. It also does not include vesicular loading and release or the contribution of glutamate to energy metabolism in neurons or astrocytes [38,44,45]. The former processes are essential for neurotransmission, and the latter processes are very likely to affect the metabolic state of the neuron, and also serve as competing processes for vesicular loading.

### C. The need for an alternative model for up and down dynamics

The above models successfully reproduce certain aspects of up and down state dynamics. However, there is a disconnect between the proposed functions of neuronal up and down states (such as synaptic plasticity, memory consolidation, cellular maintenance activities, and recovery of scarce resources), and the network mechanisms underlying the computational models generating these states. While these models do include the excitatory and inhibitory processes implied by the necessity of glutamate and GABA in experimental systems, they do not have any clear connection to plasticity, cellular maintenance, or cellular energetics. We propose that an examination of the *biochemical* properties of single tripartite synapses in a network can reveal the link between the function and mechanism of cortical bistability, and electrical properties of the synapse can be derived from basic physical and chemical principles.

We hypothesize that neuronal up and down states could be generated in part due to depletion and restoration of intracellular resources such as energy stores (ATP) and/or neurotransmitter (specifically, readily releasable neurotransmitter-containing vesicles) after prolonged neuronal firing. We thus developed a parametric “neurochemical” model of an astrocyte-presynaptic-terminal-postsynaptic-terminal-vasculature-extracellular-fluid unit, to elucidate the contribution of subcellular dynamics at the level of the tripartite synapse to the generation of up and down states. This model is *complementary* to existing models in that the primary focus is the determination of the role of biochemical processes; network processes are nevertheless absolutely essential to the development of up and down states, and are represented in the model as well. Our model is neither a phenomenological model (like the integrate-and-fire models and the models based on the Hodgkin-Huxley formalism) nor a mean-field model, and it represents a unique class of models. In this work, we demonstrate that periods of rapid firing with a

relatively depolarized resting membrane potential resembling up states in single neurons, and periods of quiescence with a relatively hyperpolarized membrane potential resembling down states in single neurons, appear due to use dependence of both ATP and releasable neurotransmitter-containing vesicles. The model reveals an intimate relationship between cellular energetics and neurotransmission at the tripartite synapse, and this interaction is shown to modulate transitions at the network level. Consideration of the interplay between cellular energetics, neurotransmission, and other processes at the cellular level may prove to be the link that connects the function and mechanism of generation of the ubiquitous up and down states.

**D. Organization of the paper**

The paper is organized in the following way: in Sec. II we give an overview of our neurochemical model. Section III demonstrates the regimes of operation of the model and how resource limitations generate the different regimes. Section IV reviews the effects of various “critical” parameters on up and down state dynamics in the model. In Sec. V we discuss the implications of resource limitation for the tripartite synapse, and we conclude with Sec. VI.

**II. OVERVIEW OF THE MODEL**

The model was developed from elementary principles of chemical reactions in the SimBio environment of MATLAB R2018b (Mathworks, Natick, MA). Because we explicitly considered nonnegligible quantities of enzyme-bound substrate, Michaelis-Menten kinetics was inappropriate. Chemical kinetic equations were written using the principle of mass balance, assuming first order in each species. Diffusion of the neurotransmitter in the synaptic cleft was approximated by including an additional compartment which functioned as a buffer for neurotransmitter molecules. Membrane potentials were calculated using elementary electrochemical principles. The model was implemented as a system of 143 ordinary differential equations representing the included chemical reactions, with a number of “rules” and “events” representing decision logic within the system (see “specification of model,” “equations,” “tables of parameters,” “rules,” and “events” in the Supplemental Material [46], which includes Refs. [6,8,9,21,44,47–71]). The model was run on a Dell 5820 workstation (Dell Computers, Round Rock, TX). The equations were solved using the ode15s solver in MATLAB, with a maximum step size of 2 ms.

We implemented a transient (time-accurate, non-steady-state) model incorporating the presynaptic terminal, postsynaptic terminal, and astrocytic component of an excitatory tripartite synapse. The primary processes modeled are depicted in Fig. 1. Processes related to neurotransmission included generation and reuptake of neurotransmitter, loading into synaptic vesicles, and transient binding at the postsynaptic terminal for signaling. Processes related to synaptic energetics included the major chemical reactions involved in the generation and utilization of ATP, the primary energy-carrying molecule used by cells. Network processes were modeled using decision logic.

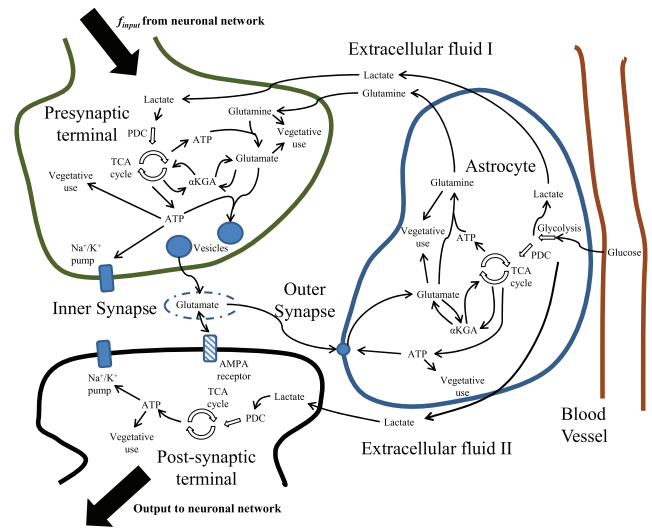


FIG. 1. Schematic of the tripartite synapse. The open arrows show significant named biochemical pathways, while thin line arrows show other reaction pathways. The “inner synapse” compartment is represented by the dotted circle, while the “outer synapse” compartment includes the rest of the synaptic cleft volume. The thick black arrows show input from and output to the rest of the neuronal network. The processes occurring in the neuronal network—summation in other neurons, ignition of the network, and extinction of the network—are modeled using decision logic. The input into the presynaptic terminal includes the summation of all signals arriving at the presynaptic neuron, and is represented by  $f_{input}$ . PDC: pyruvate dehydrogenase complex; TCA cycle: tricarboxylic acid cycle; αKGA: α-ketoglutarate.

The complete specification of the model, including assumptions, determination of parameters, implementation of ignition, and modeling of inhibition, is found in the Supplemental Material (“specification of model”) [46]. In brief, ordinary differential equations were used to calculate the concentrations of chemical species within the modeled compartments as a function of time. Kinetic rate constant parameters, which appear in the differential equations, were selected to yield close-to-physiologic values, and were not changed during simulations once determined, except in simulations specifically testing variation in one parameter. This selection of parameters was not the only possible set of parameters that could yield close-to-physiologic results.

Several “critical” parameters represent important aspects of the network in the model. These include the variable component of the input firing frequency ( $\nu$ ), the extinction parameter ( $\zeta$ ), the threshold number of filled vesicles for ignition ( $N_{critical}$ ), and the threshold concentration of ATP for extinction ( $E_{critical}$ ). Two additional “critical parameters,” the constant component of the “network” input firing frequency ( $\epsilon$ ) and the synaptic integration time constant ( $\tau_{synapse}$ ), represent properties intrinsic to the tripartite synapse. All of these parameters appear only in the decision logic of the model. Simulations varying  $\nu$ ,  $\zeta$ , and  $\epsilon$  were performed to investigate the dynamics of the model.  $N_{critical}$ ,  $E_{critical}$ , and  $\tau_{synapse}$  were held constant through all of the simulations.

Decision logic was used to determine input firing frequency from the network, and whether or not there was a

“firing” event (release of a synaptic vesicle) in the presynaptic terminal. Several “firing frequencies” were defined in the model. The quantity  $f_{\text{input}}$  represents the *instantaneous* input firing frequency arriving from the network (via summation at the axon hillock and transmission down the axon) at the presynaptic terminal. The quantity  $f_{\text{MAO}}$  (“moving average output frequency”) represents the effective output firing frequency of the presynaptic terminal, as calculated based on release of synaptic vesicles. It was calculated as a moving average over the last three firing events in order to smooth out instantaneous fluctuations related to coincidental spontaneous vesicle release. The quantity  $f_{\text{max}} = \varepsilon + \nu$  (constant component of the “network” input firing frequency + variable component of the network input firing frequency) represents the *maximum* input firing frequency arriving from the network at the presynaptic terminal. The quantity  $\varepsilon$  (constant component of the “network” input firing frequency) represents the minimum input firing frequency caused by spontaneous vesicle release [72]; this is treated the same as a “network input” although strictly speaking, as noted above, the value of  $\varepsilon$  is intrinsic to the presynaptic terminal. A synaptic terminal “firing” event (release of a synaptic vesicle) was triggered if a “virtual action potential”—calculated using  $f_{\text{input}}$ —occurred inside the time window determined by  $\tau_{\text{synapse}}$ , *and* the presynaptic terminal had at least one synaptic vesicle, *and* the presynaptic terminal had at least  $E_{\text{critical}}$  concentration of ATP.

Because of the conditions of firing in the synaptic “firing” event—specifically the requirements for sufficient filled neurotransmitter vesicles and ATP— $f_{\text{MAO}}$  serves as an indicator for the status of neurotransmitter and energy resources for the presynaptic terminal, and it will decrease if the presynaptic terminal is unable to fire because of lack of either neurotransmitter or ATP. The presynaptic terminal in the control volume is representative of the other presynaptic terminals in the network, and this is the basis for the decision logic determining extinction and ignition of the network. We defined a quantity  $\varphi = f_{\text{MAO}}/f_{\text{max}}$ , where  $\varphi < 1$  indicates decreased firing due to lack of resources in the presynaptic terminal. If  $\varphi$  drops below the extinction parameter  $\zeta$ , this serves as a surrogate for the condition that enough synapses within the network also have insufficient resources so that the network extinguishes. Network extinction causes  $f_{\text{input}}$  to drop to  $f_{\text{input}} = \varepsilon$ . Re-ignition of the network is also determined by decision logic. Initially, the network is in the quiescent (extinguished) state. If the presynaptic terminal in the control volume replenishes sufficient resources such that its number of vesicles is greater than  $N_{\text{critical}}$ , and its ATP concentration is greater than  $E_{\text{critical}}$ , this is a surrogate for enough synapses in the network replenishing sufficient resources for the network to ignite. The network ignites with the next firing event. This leads to the input frequency  $f_{\text{input}}$  increasing back to  $f_{\text{max}} = \varepsilon + \nu$ .

Extinction:

$$\varphi < \zeta \rightarrow f_{\text{input}} = \varepsilon$$

Ignition:

$$\begin{aligned} N_{\text{vesicle}} &> N_{\text{critical}} \text{ AND } ATP_{\text{presynaptic terminal}} \\ &> E_{\text{critical}} \text{ AND } \text{firing event occurs} \rightarrow f_{\text{input}} \\ &= \varepsilon + \nu. \end{aligned}$$

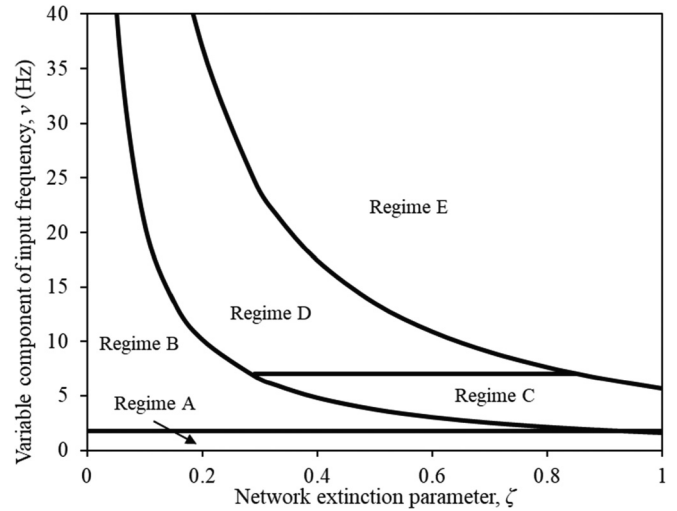


FIG. 2. Operability map revealing different operating regimes distinguished by availability of resources. Regime A shows the region wherein there are both sufficient stores of vesicles and sufficient ATP concentration for the tripartite synapse to faithfully transmit the input signal at all times. Regime B depicts the region where there is an insufficient number of vesicles for the tripartite synapse to successfully transmit the input signal continuously; however, in this regime, the system does not fulfil the criteria for the entire network to drop into the quiescent down state. Regime C shows the region where there is an insufficient number of vesicles for the tripartite synapse to successfully transmit the input signal continuously; in addition, the representative synapse’s output firing rate drops sufficiently below the input frequency such that the entire network drops into the down state, enabling the number of vesicles to recover. Regime D represents the region in which there is both an insufficient number of vesicles and a superimposed insufficient ATP concentration, which prevent the tripartite synapse from transmitting the input signal continuously. Finally, Regime E demarcates the region in which there is insufficient ATP for the tripartite synapse to continuously transmit the input signal. Regimes C, D, and E demonstrate up and down states, whereas Regimes A and B do not.

The dynamics of the model was investigated by exercising the model over a range of values for  $\varepsilon$ ,  $\nu$ , and  $\zeta$ . As noted above, the other “critical” parameters, as well as the kinetic rate constant parameters, were kept constant during these simulations. Blood glucose concentrations and the rate constant for non-neurotransmission-related ATP use (“vegetative” use) were varied for specific experiments for comparison to animal models (see Appendix B); in these simulations, all of the “critical” parameters, as well as the other kinetic rate constant parameters, were held constant.

### III. REGIMES OF OPERATION AND RESOURCE LIMITATION

#### A. Partitioning of the phase space

The firing pattern of the tripartite synapse at different frequencies demonstrates that there are different regions of operation (“regimes”). The phase space is mapped as a function of the variable component of the input frequency ( $\nu$ ) and the network extinction parameter ( $\zeta$ ) in Fig. 2. All of the other parameters are kept constant; the boundaries between

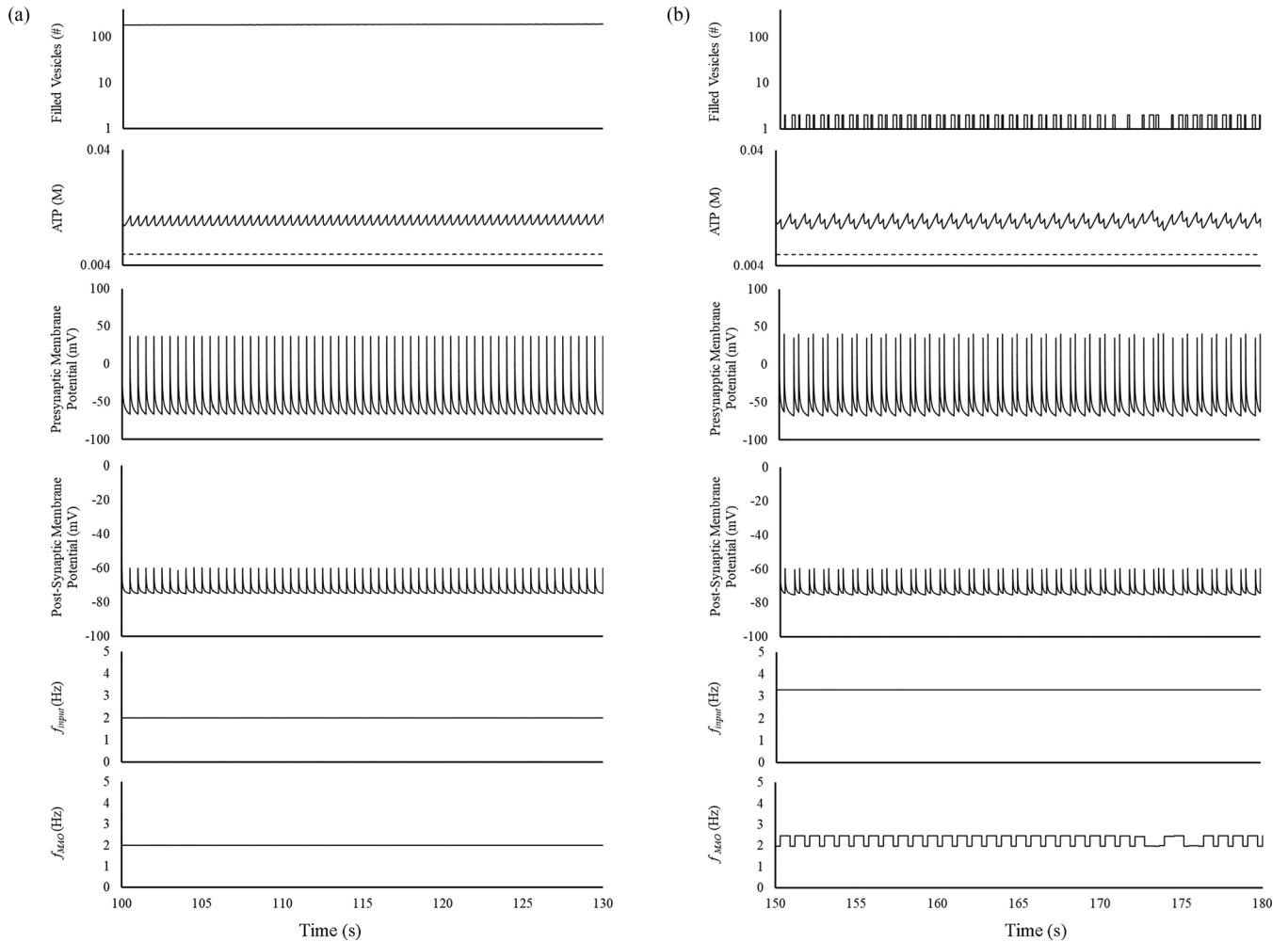


FIG. 3. Operation of the tripartite synapse without discrete up or down states. Top trace: number of filled vesicles vs time. Second trace: presynaptic ATP vs time. The dashed line represents the ATP threshold value ( $E_{critical}$ ). Third trace: presynaptic membrane potential vs time. Fourth trace: postsynaptic membrane potential vs time. Fifth trace:  $f_{input}$  vs time. Sixth trace:  $f_{MAO}$  vs time. (a) Regime A: sufficient neurotransmitter and ATP at all times.  $\epsilon = 0.3$  Hz,  $\nu = 1.7$  Hz,  $\zeta = 0.5$ . In the presence of sufficient neurotransmitter and ATP, the tripartite synapse faithfully transmits the incoming input signal. (b) Regime B: limited neurotransmitter, but system does not extinguish.  $\epsilon = 0.3$  Hz,  $\nu = 3$  Hz,  $\zeta = 0.5$ . Although there is insufficient available neurotransmitter, the system is unable to extinguish. This results in an output firing rate intermediate between  $f_{max} = \epsilon + \nu$  and  $\epsilon$ .

regimes are expected to move depending on the specific values of those parameters. Five distinct regions appear in the phase space and are distinguished by distinct patterns of dynamic behavior of the tripartite synapse, caused by differing levels of neurotransmitter and energy availability.

**B. The presence of up and down states reflects depletion of energy and neurotransmitter resources across different regimes**

We explore the connection between resource limitation and dynamics of the tripartite synapse, as a function of  $\nu$ . In a representative simulation of a lower  $\nu$  [Regime A, Fig. 3(a)], it can be seen that neither number of vesicles (top trace) nor presynaptic ATP (second trace) is significantly depleted. Because there are ample energy and neurotransmitter resources, the system never switches into a low-activity “rest” state, and there are no discrete up or down states (third and fourth traces). We describe this state as “input-limited” because  $f_{MAO}$  never takes any value other than  $f_{input}$  (fifth and sixth traces).

The behavior of the system significantly changes with higher input frequencies. With somewhat higher variable component of input frequency, the tripartite synapse transitions into Regime B [Fig. 3(b)]. In this mode, the tripartite synapse is *vesicle-limited*, in that the presynaptic terminal repeatedly runs out of vesicles (top trace). There is ample presynaptic ATP (second trace). However, although vesicles are depleted, the system cannot meet the criterion for extinction, and there are no discrete up or down states (third and fourth traces). Nevertheless, due to the shortage of vesicles, the output frequency  $f_{MAO}$  (sixth trace) does *not* equal the input frequency  $f_{input} = f_{max}$  (fifth trace).

As is seen in Fig. 4(a) (Regime C up state) and Fig. 4(b) (Regime C down state), with an intermediate high variable component of input frequency  $\nu$ , the tripartite synapse enters Regime C, and the presynaptic vesicle number oscillating between one and near 100 indicates that the system is again *vesicle-limited* (top traces). Although ATP shows significant shifts in concentration, those shifts do not impact  $f_{MAO}$

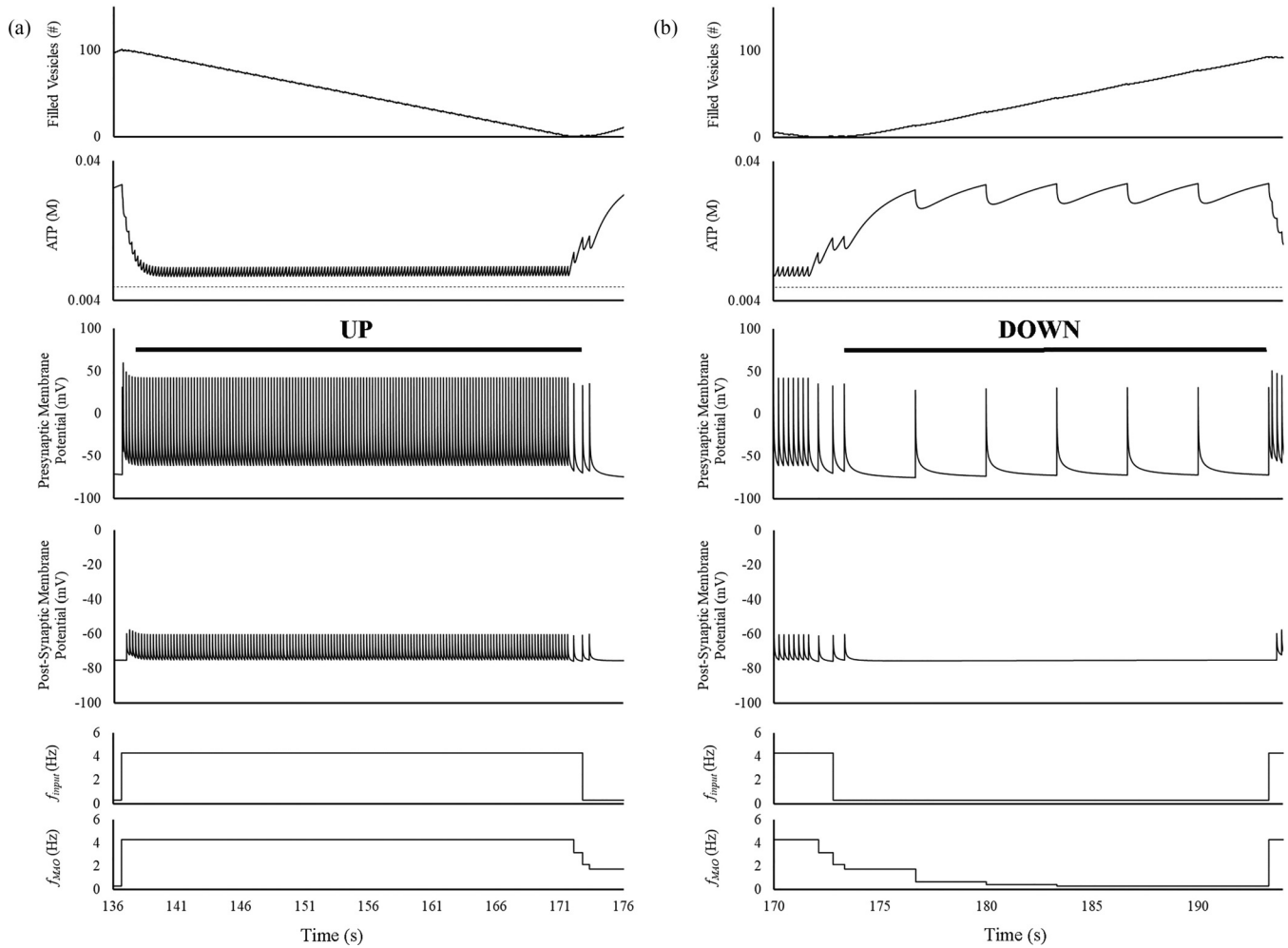


FIG. 4. Operation of the tripartite synapse with insufficient neurotransmitter, with generation of discrete up and down states: Regime C.  $\varepsilon = 0.3$  Hz,  $\nu = 4$  Hz,  $\zeta = 0.5$ . Top trace: number of filled vesicles vs time. Second trace: presynaptic ATP vs time. The dashed line represents the ATP threshold value ( $E_{\text{critical}}$ ). Third trace: presynaptic membrane potential vs time. Fourth trace: postsynaptic membrane potential vs time. Fifth trace:  $f_{\text{input}}$  vs time. Sixth trace:  $f_{\text{MAO}}$  vs time. (a) Up state: the tripartite synapse faithfully transmits the incoming input signal, such that  $f_{\text{MAO}} = f_{\text{input}} = f_{\text{max}}$ . (b) Down state: after vesicles are depleted, the output firing frequency drops sufficiently for the network to extinguish. The presynaptic terminal firing rate remains at the basal “spontaneous” rate of  $\varepsilon$ .

[Figs. 4(a) and 4(b); second trace and sixth trace]. During the downward phase of vesicle number [Fig. 4(a); top trace], the presynaptic membrane potential is more depolarized, indicating an up state (third trace). The postsynaptic membrane potential is also more depolarized (fourth trace). During the upward phase of the vesicle number [Fig. 4(b); top trace], although there is an oscillation of ATP concentration [Fig. 4(b); second trace], overall both ATP and filled vesicles are being replenished. The presynaptic membrane potential is more hyperpolarized, indicating a down state [Fig. 4(b); third trace], and the postsynaptic terminal is quiescent [though not completely silent; Fig. 4(b); fourth trace]. While the presynaptic terminal demonstrates continued spontaneous firing, most of these signals are not transmitted to the postsynaptic terminal due to a threshold effect at the postsynaptic receptors. Because of network “extinction,” the system periodically switches into a low-activity rest mode (down state), during which time both  $f_{\text{input}}$  and  $f_{\text{MAO}}$  take low values [the spontaneous frequency  $\varepsilon$ ; Fig. 4(b), fifth and sixth traces], and the presynaptic terminal

is able to recover some of its resources. After this recovery occurs, the presynaptic terminal is able to shift back into a high-activity mode for some time before switching back [Fig. 4(a); fifth and sixth traces]. Appendix A shows a representative longer term time evolution for Regime C.

In Fig. 5(a) (Regime D up state) and Fig. 5(b) (Regime D down state), the variable component of input frequency  $\nu$  is increased further, and the system enters Regime D. Again, the presynaptic vesicle number oscillating between one and near 100 indicates that the system is *vesicle-limited* [Figs. 5(a) and 5(b); top trace]. However, there is a superimposed ATP limitation during the up state—the ATP concentration oscillates around the critical value [Fig. 5(a); second trace;  $E_{\text{critical}}$ , dashed line], so that the output frequency  $f_{\text{MAO}}$  [Fig. 5(a); sixth trace] does *not* always match the input frequency  $f_{\text{input}}$  [Fig. 5(a); fifth trace]. During the downward phase of vesicle number [Fig. 5(a); top trace], the presynaptic membrane potential is more depolarized, indicating an up state [Fig. 5(a); third trace]. The postsynaptic membrane potential is also more

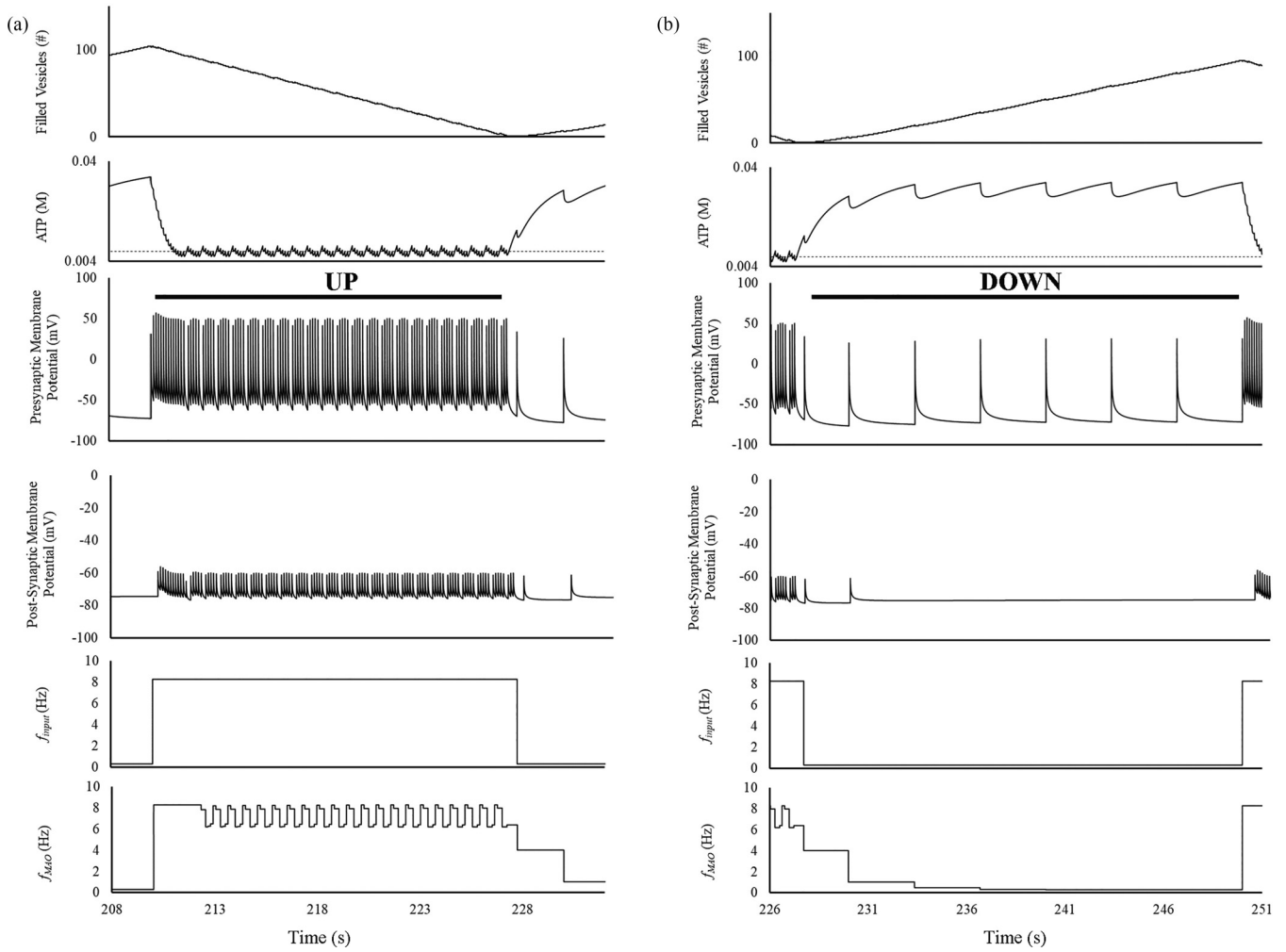


FIG. 5. Operation of the tripartite synapse with insufficient neurotransmitter and *superimposed* insufficient ATP, with generation of discrete up and down states: Regime D.  $\epsilon = 0.3$  Hz,  $\nu = 8$  Hz,  $\zeta = 0.5$ . Top trace: number of filled vesicles vs time. Second trace: presynaptic ATP vs time. The dashed line represents the ATP threshold value ( $E_{critical}$ ). Third trace: presynaptic membrane potential vs time. Fourth trace: postsynaptic membrane potential vs time. Fifth trace:  $f_{input}$  vs time. Sixth trace:  $f_{MAO}$  vs time. (a) Up state: the tripartite synapse initially faithfully transmits the incoming input signal. However, there is the appearance of a superimposed ATP limitation—leading to repetitive “misfires” of the tripartite synapse (skipping of vesicle release events). This leads to a repetitive drop in  $f_{MAO}$  to an intermediate frequency. The input frequency  $f_{input}$  does not change until the network extinguishes, which occurs when the filled vesicles are depleted, and as a result  $\varphi = f_{MAO}/f_{max}$  finally drops below  $\zeta$ . (b) Down state: after vesicles are depleted, the output firing frequency drops sufficiently for the network to extinguish. The presynaptic terminal firing rate remains at the basal “spontaneous” rate of  $\epsilon$ .

depolarized [Fig. 5(a); fourth trace]. During the upward phase of the vesicle number [Fig. 5(b); top trace], there is an oscillation of ATP [Fig. 5(b); second trace], but both ATP and filled vesicles are being replenished. The presynaptic membrane potential is more hyperpolarized, indicating a down state [Fig. 5(b); third trace], and the postsynaptic terminal is quiescent [though not completely silent; Fig. 5(b); fourth trace]. Similar to Regime C, the presynaptic terminal demonstrates continued spontaneous firing; however, most of these signals are not transmitted to the postsynaptic terminal. Because of network “extinction,” the system periodically switches into a low-activity rest mode (down state), during which time both  $f_{input}$  and  $f_{MAO}$  take low values [the spontaneous frequency  $\epsilon$ ; Fig. 5(b), fifth and sixth traces], and the presynaptic terminal is able to recover some of its resources. After this recovery occurs, the presynaptic terminal is able to shift back into

a high-activity mode for some time before switching back [Fig. 5(a); fifth and sixth traces].

Finally, Fig. 6 shows the results of increasing the input frequency even further, and the system enters Regime E. In this scenario, the availability of ATP becomes limiting—the tripartite synapse shows an *ATP-limited* mode. Although vesicle number oscillates (Fig. 6; top trace), it never drops to one. ATP is both generated and depleted rapidly (Fig. 6; second trace), leading to rapid fluctuations between depolarized up states and hyperpolarized down states in the presynaptic terminal, settling into a bursting pattern (Fig. 6; third trace). This, in turn, leads to rapid oscillations in the postsynaptic terminal membrane potential (Fig. 6; fourth trace). The output frequency  $f_{MAO}$  (Fig. 6; sixth trace) is able only to match the input frequency  $f_{input}$  (Fig. 6; fifth trace) for brief periods before the network drops into a down state.



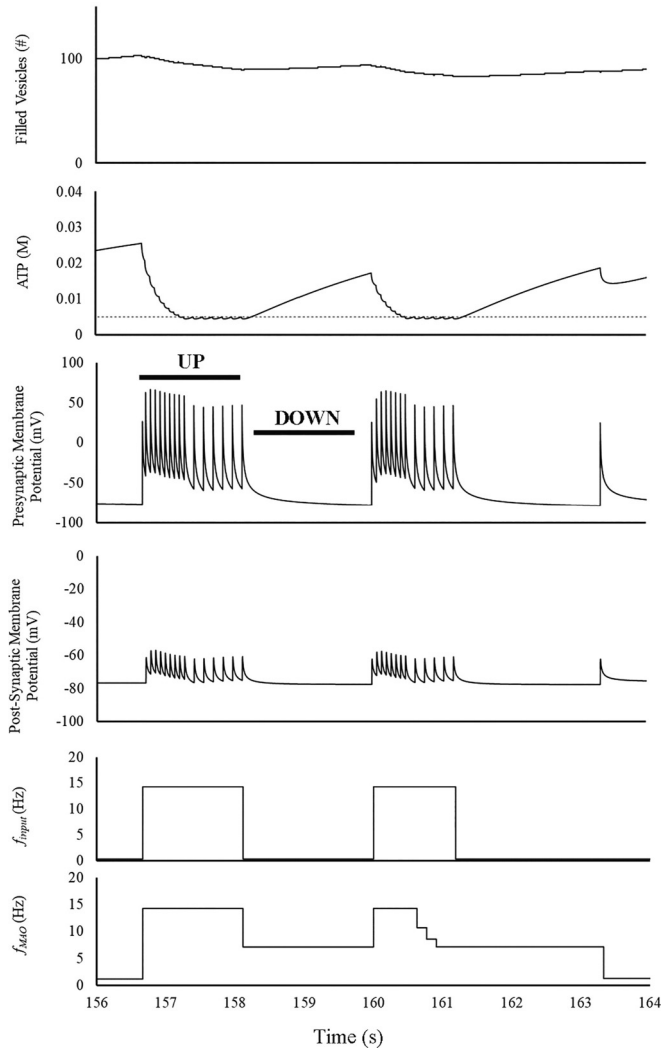


FIG. 6. Operation of the tripartite synapse with insufficient ATP, generating rapidly transitioning discrete up and down states: Regime E.  $\varepsilon = 0.3$  Hz,  $\nu = 14$  Hz,  $\zeta = 0.5$ . Top trace: number of filled vesicles vs time. Second trace: presynaptic ATP vs time. The dashed line represents the ATP threshold value ( $E_{critical}$ ). Third trace: presynaptic membrane potential vs time. Fourth trace: postsynaptic membrane potential vs time. Fifth trace:  $f_{input}$  vs time. Sixth trace:  $f_{MAO}$  vs time. During the up state, the tripartite synapse initially faithfully transmits the incoming input signal. However, it is only briefly able to sustain this rapid firing rate, prior to extinguishing. This leads to a rapid drop in the input firing frequency to the spontaneous rate ( $\varepsilon$ ), and transition into a down state. Averaging of the output frequency ( $f_{MAO}$ ) during these rapid transitions sometimes leads to the appearance of an intermediate frequency. Both the presynaptic terminal and the postsynaptic terminal take on the appearance of burst firing.

### C. *Invitro* and *in vivo* findings can be explained by fluctuations of energy and neurotransmitter resources

Because we developed our model without referring to a specific model system, we next investigated how well it tallied with empirical results from multiple *in vitro* and *in vivo* experimental systems. See Appendix B for methods of comparisons to experimental systems and detailed results. A summary of

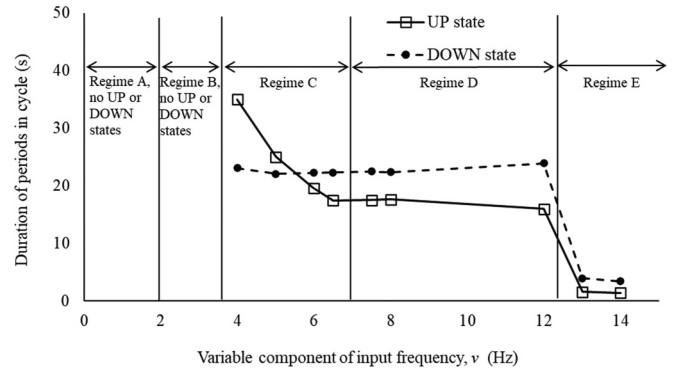


FIG. 7. Increasing the variable component of the input frequency  $\nu$  causes transitions in regimes defined by insufficient resources, leading to changes in the durations of up and down states.  $\varepsilon = 0.3$  Hz,  $\zeta = 0.5$ . Regimes A and B do not have separate up and down states. For Regimes C–E, the limit cycle durations are calculated based on the stationary state (excluding the initial transient) of the model. As  $\nu$  is increased, the tripartite synapse transitions into Regime C, where as previously shown, the output frequency is limited by the availability of neurotransmitter-filled vesicles. With further increase of  $\nu$ , the tripartite synapse transitions into Regime D, where signal transmission is limited by both neurotransmitter availability and ATP concentration. Finally, when  $\nu$  is sufficiently increased, the tripartite synapse transitions into Regime E, where signal transmission is limited by ATP availability.

the key results is found in Table I. We demonstrate that the model is capable of qualitatively matching results from six disparate experimental systems.

## IV. FREQUENCY EFFECTS ON UP/DOWN DYNAMICS

### A. Durations of up and down states decrease with increasing $\nu$

We examined the durations of the up and down states in our model as a function of the variable component of the input frequency ( $\nu$ ), maintaining all of the other parameters the same (Fig. 7). This is equivalent to “traveling” on a vertical line of constant  $\zeta$  on the operability map (Fig. 2), while varying  $\nu$ . We performed the analysis at  $\zeta = 0.5$  to investigate the behavior of the system in all five regimes. At the lowest frequencies  $\nu$ , lying within Regime A, neither neurotransmitter-filled vesicles nor ATP is limiting. With somewhat higher frequencies  $\nu$ , in Regime B, although filled vesicles are limiting, the system never reaches criteria for extinction. As a result, neither regime shows discrete up or down states. When  $\nu$  is increased further, discrete up and down states appear. The down state duration minimally changes in Regimes C and D. This occurs because the down state duration in these regimes is determined by the rate of net accumulation of vesicles, which depends on vesicle filling rate and vesicle use for spontaneous firing ( $\varepsilon$ ), and not on  $\nu$ . In Regime E, at high  $\nu$ , the duration of the down state suddenly precipitously drops, and then remains approximately stable. This is dependent on the net rate of ATP regeneration; vesicles are not significantly depleted. In contrast, there is a nearly inverse relationship between the up state duration and  $\nu$  in Regime C, following from the fact that the rate of resource depletion increases as  $\nu$  increases. In Regime D, up state duration remains roughly

TABLE I. Comparison of experimental results with model predictions.

Authors	Model	Location	Experimental system parameter change	Experimental system outcome	Corresponding neurochemical model parameter change	Neurochemical model outcome
Skrepou [73]	Mouse slice	<i>In vitro</i>	Low $Mg^{2+}$	Monotonic decrease in up state duration over time	Increase variable component of input frequency, $\nu$	Monotonic decrease in up state duration with increasing frequency
Mann, Kohl, and Paulsen [74]	Rat entorhinal cortex slice	<i>In vitro</i>	Application of GABA <sub>A</sub> receptor antagonist, gabazine	Decreasing up state duration with increased antagonist	Increase variable component of input frequency, $\nu$	Decreasing up state duration with increased frequency
Chen <i>et al.</i> [75]	Cat cortical slab	<i>In vivo</i>	Application of GABA <sub>A</sub> receptor antagonist, bicuculline	4.7–7× reduction in up state duration with addition of antagonist	Increase variable component of input frequency, $\nu$	11× reduction in up state duration with increased frequency
Huo <i>et al.</i> [76]	APP <sup>a</sup> knockout transgenic mouse	<i>In vivo</i>	Knockout of synaptic APP	Increased up state duration with decreased frequency relative to control	Decrease variable component of input frequency, $\nu$	Increased up state duration with decreased frequency within Regime C
Cunningham <i>et al.</i> [77]	Rat entorhinal cortex slice	<i>In vitro</i>	Decrease glucose in artificial extracellular fluid	Down state duration increased with reduced glucose; marginal or no change in up state duration	Decrease glucose concentration in the blood vessel compartment	Down state duration increased with reduced glucose; marginal/no change in up state duration
Castano-Prat <i>et al.</i> [78]	APP <sup>Swe</sup> /PS1 M146V/tauP301L (3xTg) mouse model	<i>In vivo</i>	Increased age of transgenic mice, leading to increased pathological protein	Both up and down state durations increased with age	Increased $k_{veg}$ (rate constant for vegetative use of ATP)	Both up and down state durations increased with increased $k_{veg}$

<sup>a</sup>Amyloid precursor protein.

constant with increasing  $\nu$ —although  $\nu$  continues to increase,  $f_{MAO}$  is capped by superimposed ATP limitation (which however does not cause extinction). There is a precipitous drop in the up state duration in Regime E, when ATP concentration becomes limiting, after which it remains roughly stable. The transitions between regimes with increasing input frequency occur due to evolving patterns of insufficient cellular energy stores and neurotransmitter in the tripartite synapse.

### B. Durations of the up state and down state change differentially with increasing $\epsilon$

We next investigated the effect of increasing the spontaneous component of the input frequency ( $\epsilon$ ) on the durations of the up and down states in our model, maintaining all of the other parameters the same (Fig. 8). We found that the duration of the up state decreases monotonically with increasing  $\epsilon$  and constant  $\nu$ , although it appears to stabilize as  $\epsilon$  continues to increase. This occurs because both neurotransmitter (filled vesicles) and energy (ATP) resources are depleted more

rapidly when the spontaneous firing rate, and thus the total input firing frequency in the up state ( $f_{input} = \epsilon + \nu$ ), is higher. In contrast, the duration of the down state initially decreases with increasing  $\epsilon$ , prior to rising again. The duration of the down state initially decreases with increasing  $\epsilon$  because a faster spontaneous firing frequency leads to ignition earlier. As  $\epsilon$  continues to increase, this effect is opposed and eventually overwhelmed by depletion of neurotransmitter (filled vesicles) and energy (ATP) resources caused by the spontaneous firing events themselves. The more rapid depletion of these resources slows down the presynaptic terminal's ability to reach the conditions for ignition, which leads to the duration of the down state rising again with higher  $\epsilon$ . There appears to be a minimum in the down state duration somewhere between  $\epsilon = 0.1$  Hz and  $\epsilon = 0.3$  Hz. Another interesting finding was that the cycle-to-cycle variability in the duration of up and down states (represented by the error bars in Fig. 8) significantly increases with decreasing  $\epsilon$ , due to increased variability in the number of filled vesicles generated in the presynaptic terminal prior to the network switching back into the up state. This occurs because the presynaptic terminal has

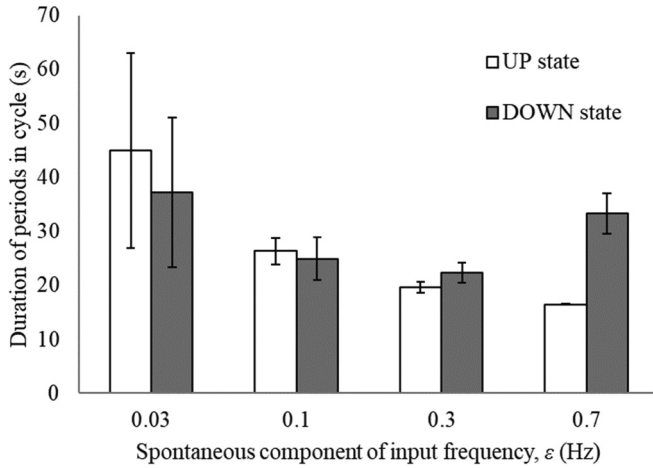


FIG. 8. Increasing the spontaneous component of the input frequency  $\varepsilon$  causes differential changes in the durations of the up and down states, due to differential effects on resource availability.  $\nu = 6$  Hz,  $\zeta = 0.5$ . The system operates in Regime C for all chosen values of  $\varepsilon$ . The error bars show the sample standard deviation of cycle duration at each  $\varepsilon$ . The duration of the up state decreases monotonically with increasing  $\varepsilon$  and constant  $\nu$ , appearing to stabilize as  $\varepsilon$  continues to increase. The duration of the down state initially decreases with increasing  $\varepsilon$ , prior to rising again.

more time to accumulate filled vesicles prior to the system reigniting into an up state with the next spontaneous firing event.

## V. DISCUSSION

### A. Synaptic up and down states, neuronal up and down states, and local field potentials

Our model demonstrates the existence of up and down states at the single synapse level, caused by network-level processes. We are not aware of any work that has directly recorded up and down states at the synaptic level; however, these have clearly been recorded at the single neuronal level, and these correlate with up and down states at both the level of local field potentials (LFPs) and slow oscillations during slow wave sleep on electroencephalography (EEG) [5]. Because an individual neuron's synapses are all connected to that neuron through the axon, we expect that synaptic up and down states should correspond very closely to the up and down states recorded from single neurons. LFPs are recorded extracellularly, and multiple current sources, including synaptic activity, action potentials, calcium spikes, other currents, afterhyperpolarizations, gap junctions, and ephaptic effects (electrical field effects caused by the presence of conductive extracellular medium) contribute to the signal through electrical superposition [79]. In addition, geometrical considerations and temporal summation determine the actual form of LFP recordings [79]. Nevertheless, summation of synaptic activity, as demonstrated in our model, contributes to the generation of both single neuronal recordings and LFPs. This implies that LFPs can serve as a reasonable surrogate for activity at the single neuronal and single synaptic level (and vice versa), and results obtained from analysis of LFPs, single neuronal intracellular recordings, and our theoretical results for single synapses are comparable.

### B. Neurotransmission and energy status are intimately related

In our model, we have focused on a glutamatergic synapse because approximately 80% of neocortical neurons use glutamate as their neurotransmitter, and approximately 85% of neocortical synapses are excitatory. The supply of glutamate for neurotransmission is thus essential for the functioning of the brain [44,80]. For a signal to be processed at a glutamatergic synapse, previously released glutamate must be removed efficiently from the synaptic cleft, and neurons must replenish their supplies of glutamate. Astrocytes, as participants in the tripartite synapse, are intimately involved in the recycling of glutamate through the glutamate-glutamine cycle: the released glutamate is mostly reuptaken by astrocytes, converted into glutamine, exported back to neurons, and then converted back to glutamate for further neurotransmission [44]. Notably, similar considerations apply to GABAergic synapses as well, although the pathway is somewhat different. In the resting human brain, the glutamate-glutamine cycle constitutes a major metabolic flux, accounting for approximately 80% of glucose oxidation [45]. Neurons are themselves also very metabolically active due to significant energy expended for maintaining and resetting the resting membrane potential for signaling [52,81]. Glutamatergic signaling thus represents a major energy expenditure for both neurons and astrocytes.

The universal energy currency for all cells is ATP. In brain tissue, ATP is produced locally through glycolysis, oxidative metabolism using acetyl coenzyme A (acetyl CoA) in the mitochondria, or through nonlocal transport of lactate produced via glycolysis in the astrocytes. This lactate is subsequently oxidized in glutamatergic terminals [82,83]. Notably, however, in addition to being the major excitatory neurotransmitter in the brain, glutamate is also used as a substrate for production of ATP [44,45]. This allows it to be a metabolic linkage between neurotransmission and energy availability in the tripartite synapse.

Functionally, then, there is competition for glutamate to be used as substrate for energy generation versus for neurotransmission. This competition becomes the biochemically based trigger for network-level changes, which in turn drive the transitions between up and down states. The lack of glutamate for either neurotransmission, or energy generation, or both, during prolonged neuronal firing provides a potential function for the state transitions: neurotransmitter and ATP stores are regenerated during down states, and up states represent brief wake-like states, similar to the concept proposed by Destexhe *et al.* [5]. It has been posited that up states switch to down states due to a fatigue mechanism such as spike frequency adaptation currents or synaptic short-term depression, and this fatigue mechanism recovers until the network switches back into the up state [1]. Either the number of vesicles, or the concentration of ATP, is inversely correlated with this "fatigue variable," depending on the regime [84]. Interestingly, depletion of readily releasable neurotransmitter-filled vesicles is one of the proposed mechanisms of short-term depression [85]. Our model exhibits the phenomenon of short-term depression due to shortage of vesicles, and even demonstrates a high-pass filtering characteristic, as shown by Rosenbaum, Rubin, and Doiron [86].

### C. *In vivo* modes of operation

The existence of multiple modes of operation begs the question “Which regime do neurons operate in *in vivo*?” This is a difficult question to answer, and it is likely that neurons in different parts of the brain operate in different regimes at different times, depending on the computational demands of that region of the brain. What likely occurs is that synapses function in one of the above regimes until they can no longer be supplied sufficient raw resources (i.e., glutamine, glucose, and other nutrients necessary for function), then they drop into a further low state of function until they can recover those resources. This adds another layer of use-dependence, which has been seen *in vivo* (for example, see Vyzovskiy *et al.* [3]). One intriguing possibility is that neurons function in one of the regimes that allow brief bursts of extremely high-frequency activity (Regime D or E), as an adaptive mechanism for organisms to quickly respond to rapidly changing stimuli in the environment (such as the appearance of a predator). Since this sort of stimulus that needs to be rapidly processed is relatively uncommon, the organism can “afford” to use up all of its neuronal resources briefly in order to survive the situation and recovers those resources by local and global (behavioral) sleep.

### D. Physiological insights from experimental systems: A final common pathway?

We compared the predictions of our model regarding durations of the up and down states to six disparate experimental models, and found that our results qualitatively matched the results of those studies without changing any parameters other than those that were varied in the experimental models. Furthermore, we found that transition to Regime E was the final common pathway for resource failure in several different pathological states. Our model thus leads us to the following testable hypotheses:

(1) Mechanisms leading to increased firing rate, such as increased concentrations of glutamate receptor agonists, GABA<sub>A</sub> receptor antagonists, or even high-frequency electrical stimulation, will lead to operation of the tripartite synapse in Regime E.

(2) Severely decreased flux through the TCA cycle will lead to operation of the tripartite synapse in Regime E.

(3) Increased non-neurotransmission-related use of ATP, such as in the context of severe proteinopathy, will lead to operation of the tripartite synapse in Regime E.

(4) More speculatively, mitochondrial toxins, such as poisons affecting the electron transport chain, or toxins causing disruption of the proton gradient, will lead to operation of the tripartite synapse in Regime E.

Synthesizing our findings, we speculate that severe enough energy deprivation can lead to rapid cycling of up and down states, regardless of initial cause, and this may be a single-synapse neurochemical correlate of seizures. Furthermore, this occurs even without the presence of glutamatergic excitotoxicity, which would be expected to make the situation worse. Notably, however, it may be that cell death occurs prior to the appearance of this final common pathway, in some circumstances.

### E. Up and down states and “local sleep”

Sleep was previously viewed as an “all-or-none” phenomenon: either an organism was asleep, or it was not [87]. However, this view has more recently been challenged by multiple findings suggesting that sleep phenomena, such as slow wave oscillations of sleep and their underlying neuronal up and down states, occur locally and may occur even during non-slow-wave-sleep states—a phenomenon that has been called “local sleep.” It has been proposed that such “local sleep” is use-dependent: specifically, that sleep serves a function in synaptic plasticity, and since plasticity is a local process, so too is (local) sleep [88]. Several studies, including [89–91], have shown that slow wave sleep can be altered in a use-dependent fashion in humans, and other studies such as [92] have correlated local slow wave sleep with underlying local up and down state oscillations. It was subsequently shown that such local changes in slow wave sleep can occur in a use-dependent fashion and correlate with the development of neuronal up and down states in rats [3]. A different line of evidence shows that brain metabolism, as measured by the cerebral metabolic rate of oxygen (CMRO<sub>2</sub>), significantly decreases during slow wave sleep [93,94]. Thus, there may be a correlation between use-dependent increases in slow wave sleep and decreased brain metabolism in the same regions. This is an intriguing association, and suggests that further studies could investigate the changes in brain metabolism that occur during use-dependent local sleep. Our model directly demonstrates use-dependent state transitions that are driven by utilization of cellular resources, and are caused by network-level processes. It suggests that two major classes of theories of sleep—that sleep is to maintain synaptic connectivity (a network-level explanation), and that sleep is to restore cellular resources (a cellular-level explanation) could be unified through this biochemical-network interaction. It has been pointed out that these two classes of theories are not mutually exclusive and that “sleep could be a cellular property precisely because the cell’s biochemistry, including its metabolism, is driven by network activity” [95].

### F. Limitations

Our model does present some limitations. We have modeled network processes using a small set of parameters:  $\nu$ ,  $\zeta$ ,  $E_{\text{critical}}$ , and  $N_{\text{critical}}$ . One limitation is that these parameters may not always be straightforward to determine. The variable component of the input frequency  $\nu$  is relatively easy to conceptualize, but hides the rich interaction of dendritic inputs required to create the effective firing frequency. This limitation could be ameliorated by including the other compartments of the presynaptic neuron: dendrite, soma, and axon. The network extinction parameter  $\zeta$  encapsulates multiple network features, and is dependent on multiple factors including network-level factors such as the structural and effective connectivity of the network, as well as cellular-level factors such as the metabolic characteristics of the individual neurons in the network (which are generally inhomogeneous populations). The relationship between  $\zeta$  and these factors is unclear, and at least initially, the value of  $\zeta$  for a particular network would likely have to be empirically determined by the behavior of the network. The biochemical parameters  $E_{\text{critical}}$

and  $N_{\text{critical}}$  are threshold values in the presynaptic terminal of interest, which determine the behavior of the network. These both are also dependent in unclear ways on the network-level and cellular-level factors listed above, and similarly would likely be empirically determined for real neuronal networks.

Another related limitation is the use of decision logic for whether the presynaptic terminal fires or not, and whether network firing “ignites” or “extinguishes” in our model. There is no module inside a presynaptic terminal which “decides” whether or not to fire by evaluating whether there are enough resources available to it, nor does the network as a whole “decide” whether to fire at a low or high rate. Rather, these are determined purely by biochemical thermodynamic processes and reaction kinetics. While it is theoretically possible to represent all of these processes with differential equations, there are an overwhelming number of reactions occurring in real cells, and modeling all of these reactions is likely beyond the capability of current computers. In addition, because the extra competing reactions are not modeled in reduced realistic models, the kinetic parameters that would result in realistic model behavior are very likely not going to be the same as those which would be measured in the real system. This limits the ability to reproduce realistic results in the model using empirically derived kinetic parameters—a problem which is not encountered in more abstract phenomenological models.

## VI. CONCLUSIONS

We have demonstrated a model of the tripartite synapse based on biochemistry, which encompasses the presynaptic terminal, postsynaptic terminal, astrocytic process, and blood vessel, derived entirely from elementary principles. Electrical properties, specifically the calculation of the membrane potential, are also based purely on first principles. The model focuses on the biochemical processes occurring in the tripartite synapse, including synaptic vesicle loading and release, while still modeling essential network processes, making it complementary to existing network integrate-and-fire models and models based on the mean field formulation. Our model connects neurotransmission and energy generation through the competing uses of glutamate as substrate for each process, and unlike other models, includes energy-utilizing processes that are not directly related to neurotransmission (“vegetative” processes). It qualitatively matches six disparate experimental systems, including the alteration of up and down states in the presence of low magnesium, in the presence of GABA<sub>A</sub> receptor antagonist (leading to increased excitation; two models), with decreased firing rate due to changes in synaptic protein expression, with varying amounts of glucose, and with increased load of vegetative processes, without requiring changes to the parameters utilized, other than those associated with each experimental condition. It establishes a likely mechanism for the concept of “fatigue variables” leading to state transitions, and also demonstrates a possible explanation (an ignition phenomenon) for the findings that the states of single neurons can determine the state of a network. With this model, we demonstrate that biochemical processes within neuronal networks can directly affect the network-level behavior of the system, and provide a possible mechanism-function link for

the generation of neuronal up and down states. The interactions between these biochemical processes may underlie the phenomenon of “local sleep.” Resource limitation may lead to a final common pathway of synaptic firing patterns. Ultimately, sleep-like behavior may be a fundamental property of networks of tripartite synapses.

The data that support the findings of this study are available upon reasonable request from the authors.

## ACKNOWLEDGMENTS

S.N.J. conceived and designed the study. S.N.J. performed and A.N.J. contributed to the literature review. A.N.J. and N.D.J. designed the model and performed data analysis. A.N.J. wrote the first draft of the manuscript, and S.N.J. wrote sections of the manuscript. All authors contributed to manuscript revision and read and approved the submitted version. A.N.J. is a nonremunerated member of the board of directors of the American Society for Experimental Neurotherapeutics. S.N.J. and N.D.J. declare that they have no potential conflicts of interest with the contents of this article. This work is not funded by any funding agency, organization, or outside individual. The National Center for Adaptive Neurotechnologies is supported by BTRC Grant No. 1P41EB018783 from the NIBIB, National Institutes of Health.

## APPENDIX A: REPRESENTATIVE TIME EVOLUTION OF A REGIME

The time evolution of a representative simulation is shown in this section. Each simulation run had a “starting transient” which lasted up to approximately 50 sec, which was not included in the analysis. After this starting transient, each regime showed steady behavior. In the representative simulation, in which the system is in Regime C, distinct up and down states are seen, as indicated by clearly distinct resting membrane potentials (Fig. 9). Regime C is also a “vesicle-limited” mode, and in this regime, the output frequency of the representative synapse does drop sufficiently (due to lack of available vesicles) to cause the network to “extinguish.” Network signal “extinction” leads to a down state in the representative tripartite synapse, allowing it to replenish its stores of both releasable vesicles and ATP. When the amounts of both resources surpass a specific threshold, the network “ignites” again to go into an up state. In this regime, the tripartite synapse is able to faithfully transmit signal (i.e., match the input frequency) for the entire up state. This alternation of up and down states persists to the end of the simulation.

## APPENDIX B: COMPARISON TO EXPERIMENTAL SYSTEMS

### 1. Considerations for a computational neurochemical model

The presence of a large number of degrees of freedom in realistic biophysical models, such as ours, has been noted previously by Bhalla and Bower [96]. These authors also noted that for well-described systems (in their case, mitral

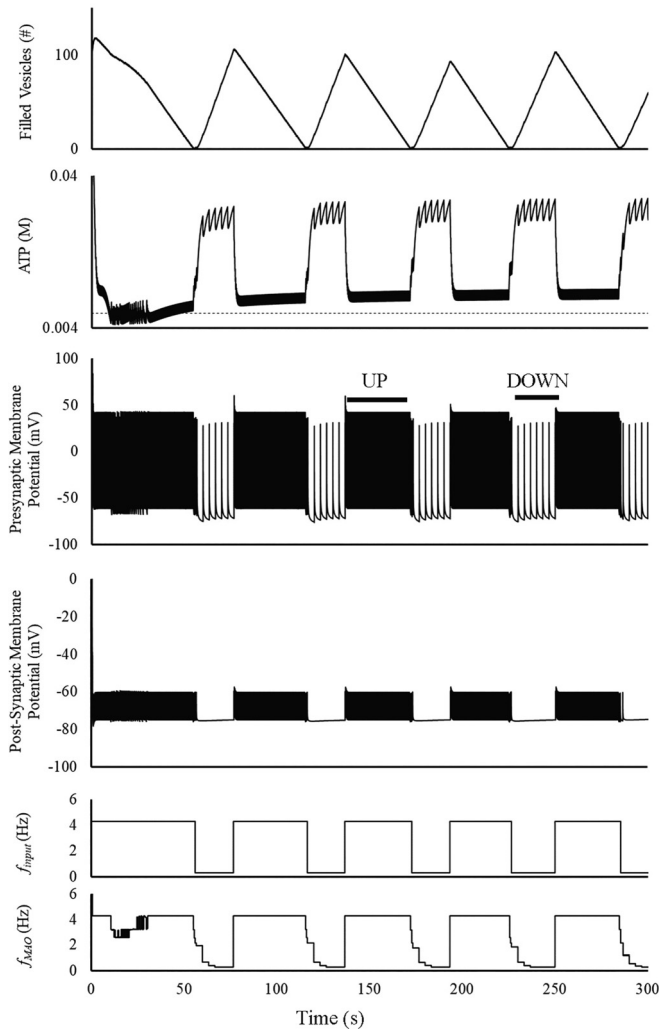


FIG. 9. Time evolution of Regime C demonstrates cyclical alternation between up and down states.  $\epsilon = 0.3$  Hz,  $\nu = 4$  Hz,  $\zeta = 0.5$ . Top trace: number of filled vesicles vs time. Second trace: presynaptic ATP vs time. Third trace: presynaptic membrane potential vs time. Fourth trace: postsynaptic membrane potential vs time. Fifth trace:  $f_{\text{input}}$  vs time. Sixth trace:  $f_{\text{MAO}}$  vs time. During an up state, the vesicle number rapidly drops, and the representative tripartite synapse reaches the criterion for “extinction” ( $\varphi = f_{\text{MAO}}/f_{\text{max}} < \zeta$ ). This signals the network to drop into a low-activity state— $f_{\text{input}} = \epsilon$ . When this occurs, the representative tripartite synapse drops into a low-activity mode—the down state—and because of the low firing activity, the vesicle pool and ATP concentrations are allowed to replenish. After meeting ignition criteria, the network is imputed to have sufficient resources for spontaneous firing of component synapses to “reignite” the network, leading to the high-activity state—the up state. The cycle then repeats.

cells of the olfactory bulb), even realistic models with many parameters can be constrained by experimental data, and only one set of parameters in the parameter space may fit that data. On the other hand, for less-well-known systems (granule cells of the olfactory bulb in their work), there may be several regions within the parameter space that can successfully reproduce the experimental data. In this situation, they stated both that experimental data are necessary to constrain model parameters, and that there is utility in

“careful studies of parameter space [from the model] as a guide to future experimental work” [96]. Of note, most current models are designed to match one specific dataset, whereas we are qualitatively matching multiple disparate experimental datasets with one model. The parameters in our model may be adjusted to more closely match an individual dataset.

However, there are several caveats to note. One important consideration is that even with a complex model such as ours, not all of the processes in the real cell are modeled—for instance, we excluded reaction pathways such as the pentose phosphate pathway, and fatty acid synthesis and oxidation. These pathways *do* exist in real cells, and even if kinetic parameters are measured empirically, they may be different than what is needed for the model to closely replicate the empirical data, because there is competition for substrate with the additional unmodeled pathways. Another caveat is that the kinetic parameters likely vary between species, and may vary within species, or even within a specific individual (based on the region assessed, the time assessed, or the state of the organism). Finally, the experimental procedures themselves may alter the measurement of the model parameters. If, for instance, an inhibitor is used to block a competing pathway in order to measure a kinetic rate constant, there is no way to know whether that inhibitor also has off-target effects. These issues make fitting empirical data to a simplified but realistic model an approximate art at best.

**2. Increasing input frequency leads to resource limitation, causing significant decreases in the durations of up states, similar to those seen in two *in vitro* cortical slice experiments**

In an *in vitro* slice model from young and adult mice, Skrempou [73] examined differences in seizure threshold from neocortical and hippocampal (CA3) tissue. It was demonstrated that in the presence of low magnesium, the duration of up states in the slices progressively decreases over time. It is hypothesized that epileptiform activity develops in low magnesium conditions due to the gradual release of the  $\text{Mg}^{2+}$  blockade of the excitatory N-methyl-D-aspartate (NMDA) glutamate receptor. This release of excitation corresponds to an increased firing frequency in our model. We found that the up state durations in Regimes C, D, and E corresponded well with Skrempou’s [73] “control” condition (normal magnesium), and “early” and “intermediate” periods after applying low magnesium conditions, respectively (Fig. 10). Skrempou did not investigate the effects of low magnesium on the duration of down states [73].

Mann, Kohl, and Paulsen [74] evaluated the roles of GABA<sub>A</sub> receptors in persistent cortical activity in another *in vitro* slice model from young rat entorhinal cortex. They showed that the up state duration monotonically decreased with increasing concentration of the GABA<sub>A</sub> receptor antagonist gabazine. An increasing concentration of GABA<sub>A</sub> receptor antagonist corresponds with an *increase* of the firing frequency in our model, and we also found a monotonically decreasing up state duration with increasing firing frequency in the transition from Regime D to Regime E (Fig. 11). Mann, Kohl, and Paulsen did not investigate the effects of gabazine on the duration of down states [74].

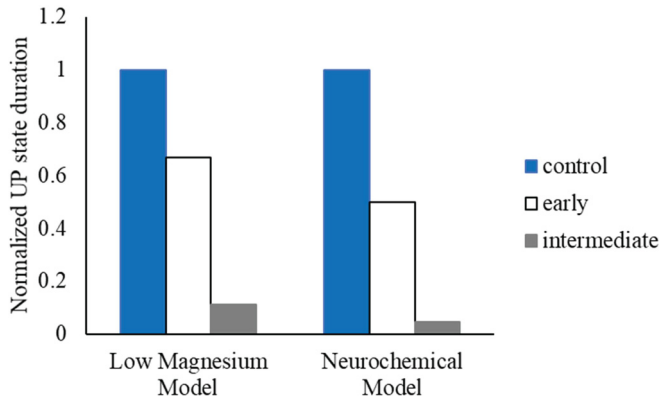


FIG. 10. Up state duration decreases with increasing firing frequency (due to release of blockade of excitation) in an experimental system, as predicted by our model. The normalized duration of the up state decreased progressively with time in the experimental model by Skrepmpou [73] after the removal of magnesium ions from the extracellular medium, which was thought to be due to facilitation of excitation by releasing the  $Mg^{2+}$  blockade of NMDA receptors. This leads to an increased neuronal firing rate. Our model demonstrates a similar significant decrease in the duration of the up state with a transition from Regime C, to Regime D, to Regime E. We chose a representative frequency ( $\nu = 4$  Hz) from the lower end of Regime C, a representative frequency ( $\nu = 6.5$  Hz) within Regime C near the border with Regime D, and a frequency at the lower end of Regime E ( $\nu = 13$  Hz), to demonstrate this result.

### 3. Increasing input frequency leads to resource limitation, causing significant decreases in the durations of up states, similar to those seen in an *in vivo* cortical slab experiment

Chen *et al.* [75] investigated the “network dynamics in the extreme case of a complete blockage of inhibition” in a cortical slab model in cats. To examine this, they applied a different GABA<sub>A</sub> receptor antagonist, bicuculline, to the slab preparations. Although they did not evaluate concentration-dependent differences, they did show a significant drop in duration of the “active state” by 4.7–7 fold with application of bicuculline. Our model also demonstrated a large decrease in up state duration by approximately 11 fold with transition from Regime C (intermediate  $\nu$ ) to Regime E (high  $\nu$ ). Chen *et al.* did not investigate the effects of bicuculline on the duration of down states [75].

### 4. Decreasing input frequency leads to increased resource availability, causing prolonged up states and down states of unchanged duration, similar to those seen in an *in vivo* experiment

Huo *et al.* [76] noted that amyloid precursor protein (APP) is present in both presynaptic and postsynaptic terminals, and is critical for synaptic plasticity. They observed that while much attention has focused on the pathological significance of APP, much less is known about the physiological function of the protein. As such, they examined how presence or absence of APP could alter network activity, as assessed by changes in up and down state oscillations. In an *in vivo* mouse model, they demonstrated that in APP knockout mice (APP<sup>-/-</sup> mice), the duration of up states

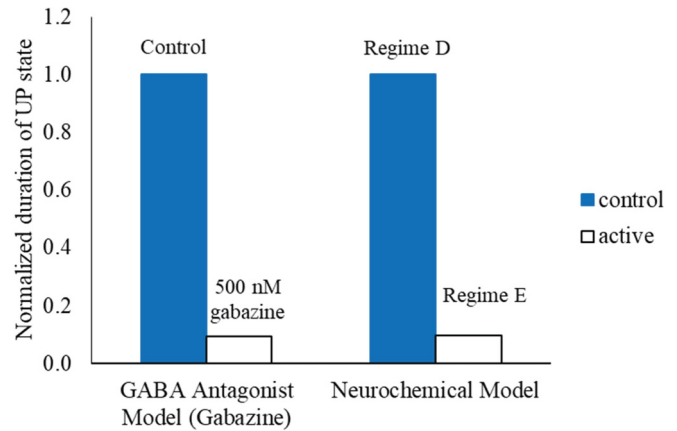


FIG. 11. Up state duration decreases with increasing firing frequency (due to blockade of inhibition) in an experimental system, as predicted by our model. The normalized duration of the up state decreases significantly in the experimental model by Mann, Kohl, and Paulsen [74] with the addition of a high concentration of GABA<sub>A</sub> receptor antagonist, which increases the excitability of the system by decreasing the inhibition. This, in turn, leads to an increased neuronal firing rate. Our model demonstrates a similar significant decrease in the duration of the up state with a transition from Regime C or Regime D to Regime E. We chose a representative frequency ( $\nu = 12$  Hz) at the higher end of Regime D, and a frequency at the lower end of Regime E ( $\nu = 13$  Hz), to demonstrate this result.

increased significantly compared to their wildtype littermates. In addition, the number of action potentials per up state decreased in APP knockout mice compared to wildtype (although not reaching statistical significance). In contrast, the down state duration was nearly identical in the two conditions. Our model qualitatively replicates these findings, with the average number of action potentials per active up state from Huo *et al.* corresponding to the firing frequency in our model. In Fig. 12(a), we show a decrease in the normalized firing frequency comparable to that in Huo *et al.*’s experimental condition (APP knockout mice). With the specific decrease in firing frequency chosen (from 6.5 Hz to 5 Hz), our model shows a prolongation in the up state duration comparable to that seen in Huo *et al.*’s work [Fig. 12(b)]. The down state duration did not appreciably change in our model (see also Fig. 7).

### 5. The duration of the down state, but not the up state, increases with decreasing concentrations of glucose, similar to an *in vitro* cortical slice experiment

We next examined the effect of changes in the boundary condition of the concentration of glucose present in the blood vessel in our model, maintaining all of the other parameters the same. Although the concentration of glucose in the blood vessel was held constant (see Assumptions in “specification of model,” Supplemental Material [46]), using a different value of blood glucose concentration changed the time evolution of the model, because the modeled reactions utilized first-order kinetics with mass balance. We found that as the boundary condition concentration of glucose, which supplies substrate for both ATP generation and

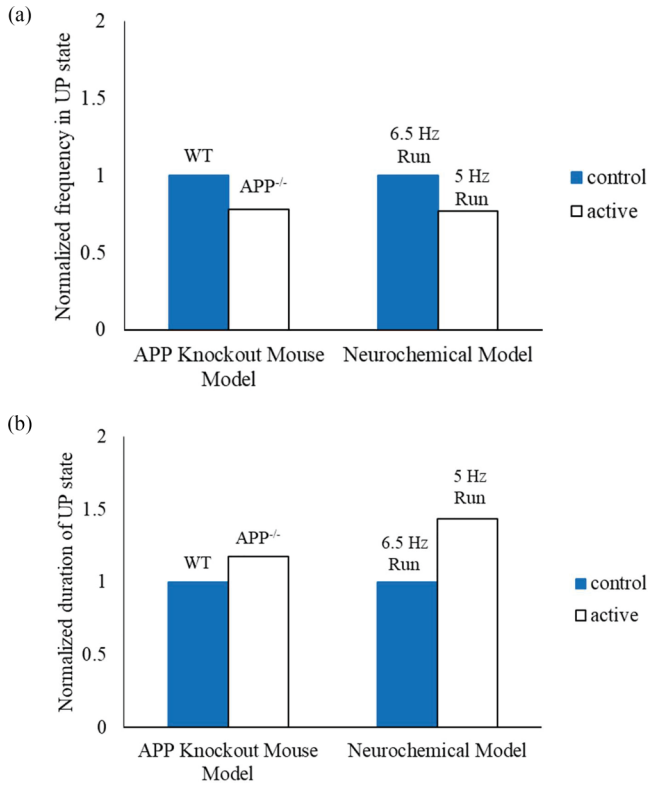


FIG. 12. Up state duration increases with decreasing firing frequency in an experimental system, as predicted by our model. (a) The normalized frequency in the up state decreases in the experimental system of Huo *et al.* [76] in the active state (APP knockout mouse, APP<sup>-/-</sup>) compared to the control (wild-type, WT). Based on the data depicted in Fig. 7, we chose a frequency (6.5 Hz) within Regime C (near the border with Regime D) to represent the control state, and another frequency (5 Hz) within Regime C to represent the active state, such that the fold change in frequency is similar to that seen in the experimental system. (b) The normalized duration of the up state increases in the experimental system in the active state (APP knockout mouse) compared to the control (WT). In our model, using the same frequencies as in (a), the normalized duration of the up state increases in the active condition compared to control, similar to the experimental model.

neurotransmitter synthesis, was decreased, initially the up state duration remained roughly constant, but the down state duration significantly increased (Fig. 13). Cunningham *et al.* [77] studied an *in vitro* model using rat entorhinal cortical slices and found that slow-wave oscillations in the slices were dependent on their metabolic states. More specifically, they found that the down state durations were significantly longer at lower glucose concentrations, with roughly stable up state durations, just as was seen in our model. We compared normalized values of glucose concentration versus normalized down state duration, and found a similar increase in normalized down state duration with decreasing normalized glucose concentration in both the empirical system and our model (Fig. 14). When we further decreased the glucose concentration in our model, we found that there was a sudden drop in both the up and down state durations (Fig. 13).

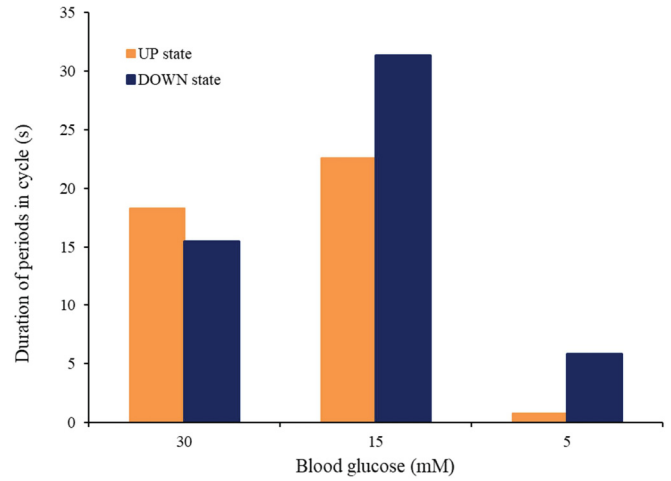


FIG. 13. Concentration of blood glucose, which serves as substrate for both energy generation and neurotransmitter synthesis, affects the duration of up and down states.  $\epsilon = 0.3$  Hz,  $\nu = 7$  Hz,  $\zeta = 0.5$ . Glucose supplies both the substrate for neurotransmitter (glutamate) and energy (ATP) generation in the tripartite synapse. As the availability of glucose decreases, the availability of both neurotransmitter and ATP decreases. This initially causes an increase in the durations of the down state; the duration of the up state stays roughly constant. As the glucose concentration continues to drop, the durations of the up and down states suddenly drop, indicating transition into Regime E with ATP limiting signal transmission in the tripartite synapse.

**6. The durations of both the up and down states increase with increasing “vegetative” use of ATP, representing an additional sink for energy resources, similar to an *in vivo* model of neurodegeneration**

As noted in “specification of model” in the Supplemental Material [46], “vegetative” functions in the cell include transcription, protein synthesis, and other “housekeeping” processes not directly related to neurotransmission or energy generation. In neurons, one such set of ATP-dependent cellular processes is the refolding or disposal of misfolded proteins, mediated by heat-shock proteins, the ubiquitin proteasome machinery, and autophagy [97–100]. These systems are upregulated, and likely overwhelmed, in a variety of neurodegenerative diseases such as Alzheimer’s disease, due to increased loads of misfolded proteins, leading these diseases to be classified as “proteinopathies” [101]. As such, neurodegenerative diseases are appropriate models for systems where the “vegetative” use of ATP is increased, representing an additional sink for energy resources. In an anesthetized triple transgenic mouse model of Alzheimer’s disease (APP-Swe/PS1M146V/tauP301L, called a 3xTg mouse model), Castano-Prat *et al.* [78] found that the down state duration increased and the up state duration showed a trend to increase in only the transgenic mice at 20 months of age, but not control mice. Importantly, while younger transgenic animals (7 months) did have intracellular A $\beta$  immunoreactivity, the older mice (20 months) had significantly worse pathology with presence of A $\beta$  plaques and neurofibrillary tangles throughout the neocortex, suggesting a significantly worse load of misfolded proteins.



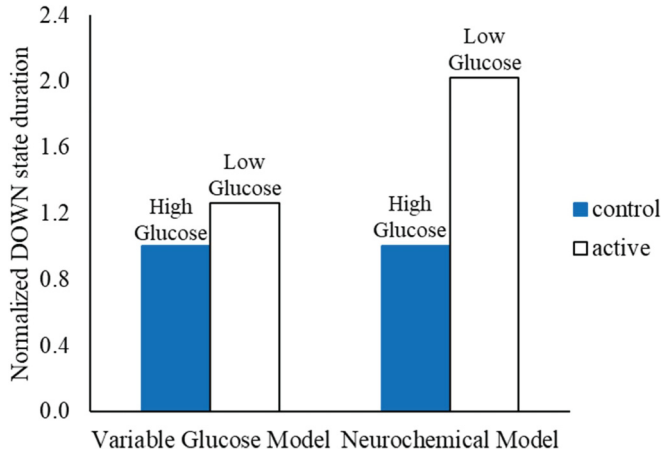


FIG. 14. Down state duration increases with decreasing glucose concentration in an experimental system, as predicted by our model. The normalized duration of the down state increases significantly in the experimental model by Cunningham *et al.* [77] with decreasing glucose concentration in the artificial cerebrospinal fluid (aCSF). This is replicated in our model with decreasing glucose concentration (using the same change in glucose concentration as depicted in Fig. 13).

We explored the effects of an increased “vegetative” use of neuronal ATP in our model by increasing the rate constant for neuronal vegetative processes in the presynaptic terminal, with all other parameters held constant. When the “vegetative” use of neuronal ATP was increased moderately, we found that *both* the up state and down state durations increased, although the down state duration increased more compared to the up state duration (Fig. 15). This is similar to the findings of Castano-Prat *et al.* [78] for both the up state duration [Fig. 16(a)] and the down state duration [Fig. 16(b)]. When the “vegetative” use of neuronal ATP was increased further in our model, again the up and down state durations significantly decreased (Fig. 15).

## 7. Methods for comparison to experimental systems

### a. Comparison of our model vs Skrepmpou [73]

Figure 2 from Skrepmpou [73] was evaluated. Values for the durations of the up state from adult and young mice in the control condition (normal concentration of magnesium) were obtained from the text. Data from the primary somatosensory cortex of the whiskers in adult mice were selected for further analysis (Fig. 2C, left panel, from Skrepmpou [73]), as trends were similar in both primary somatosensory cortex and primary motor cortex in both adult and young mice. Data points for up duration (s) in the primary somatosensory cortex of the whiskers from adult mice were measured using the measuring tool in Adobe Acrobat DC (Adobe, San Jose, California), and the depicted data points were measured with a precision of 0.01 inches. These values were then scaled by the measured distances between the labeled marks on the figure axes to obtain numerical values for up state durations. The up state durations were normalized by the up state duration of the control condition.

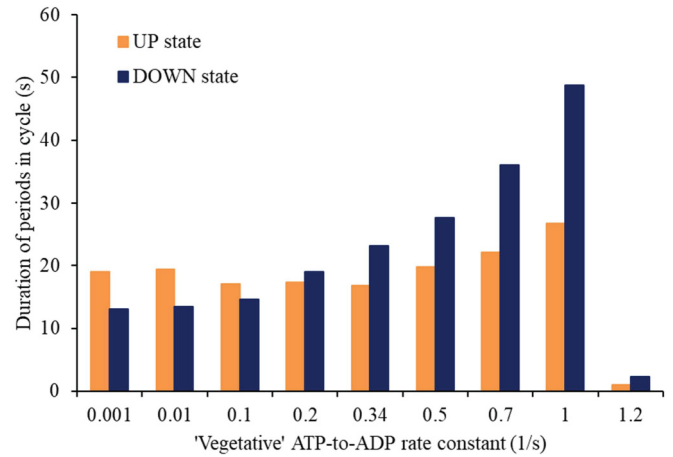


FIG. 15. Increasing non-neurotransmission-related ATP uses, representing additional sinks of energy resources, affect duration of up and down states.  $\varepsilon = 0.3$  Hz,  $\nu = 7$  Hz,  $\zeta = 0.5$ . Non-neurotransmission-related ATP uses encompass numerous processes such as transcription, translation, cellular signaling, cellular maintenance, and cellular recovery/repair processes. These are collectively represented as “vegetative” processes. As ATP use in “vegetative” processes increased, initially the durations of both the up and down states increased. With further increase, the durations of the up and down states suddenly dropped significantly, representing a transition into Regime E, where signal transmission is limited by the absence of sufficient ATP.

We then obtained equivalent data from our model. We compared simulations with the following critical parameters kept constant:  $\varepsilon = 0.3$  Hz,  $\zeta = 0.5$ ,  $\tau_{\text{synapse}} = 25$  ms, glucose = 0.02 M. The variable component of input frequency was set at  $\nu = 4$  Hz as a representative value at the lower end of Regime C;  $\nu = 6.5$  Hz as a representative value within Regime C near the border with Regime D; and  $\nu = 13$  Hz as a representative value at the lower end of Regime E. The up state durations were then normalized by the up state duration at  $\nu = 4$  Hz. These results were then plotted against those obtained from Skrepmpou [73].

### b. Comparison of our model vs Mann, Kohl, and Paulsen [74]

Figure 2 from Mann, Kohl, and Paulsen [74] was evaluated. The duration and mean interspike interval during up states with differing concentrations of GABA<sub>A</sub> receptor antagonist were obtained from the text. These were associated to obtain duration of up state as a function of mean interspike interval. The duration of up states was normalized by the duration of the up state with no GABA<sub>A</sub> receptor antagonist.

We then obtained equivalent data from our model. We compared a simulation within Regime D ( $\nu = 12$  Hz) and a simulation within Regime E ( $\nu = 13$  Hz). Because  $\tau_{\text{synapse}}$  limits the maximum frequency the model can run at ( $1/\tau_{\text{synapse}} = \nu_{\text{max}}$ ; with  $\tau_{\text{synapse}} = 25$  ms,  $\nu_{\text{max}} = 40$  Hz), testing a frequency of  $\nu = 98$  Hz would be outside of the valid bounds for the model; our model shows that there was not much difference in up state duration beyond  $\nu = 13$  Hz (data not shown). We calculated the normalized up state duration for Regime E ( $\nu = 13$  Hz,  $\varepsilon = 0.3$  Hz,  $\zeta = 0.5$ ,  $\tau_{\text{synapse}} = 25$  ms, [glucose] = 0.02M), taking Regime D ( $\nu = 12$  Hz,  $\varepsilon = 0.3$

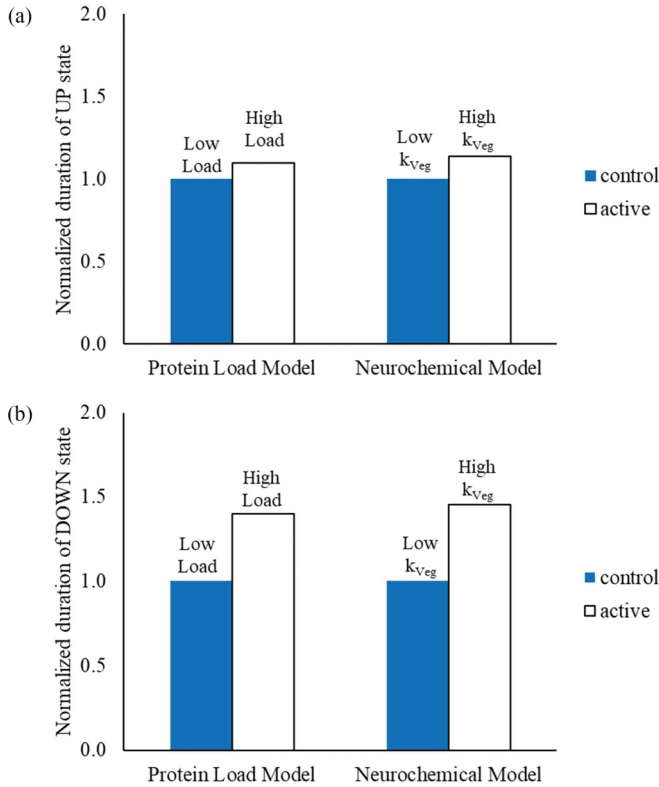


FIG. 16. Both up and down state durations increase with increasing “vegetative” use of ATP (due to increased protein load) in an experimental system, as predicted by our model. (a) The normalized duration of the up state increased in the experimental model by Castano-Prat *et al.* [78]. Increasing age in the 3xTg mouse model has been associated with increased burden of A $\beta$  plaques and neurofibrillary tangles, the presence of which implies upregulation of ATP-requiring processes to attempt to degrade the misfolded proteins. This finding is replicated in our model with increasing “vegetative” use of ATP, indicated by the rate constant for “vegetative” processes ( $k_{veg}$ ). The value of  $k_{veg}$  was set at 0.2 for the “low” protein load, and 0.5 for the “high” protein load. (b) Similarly, the normalized duration of the down state increased in both the experimental model by Castano-Prat *et al.* [78] and our model.

Hz,  $\zeta = 0.5$ ,  $\tau_{synapse} = 25$  ms, [glucose] = 0.02 M) as “control.” These values were then plotted against those obtained by Mann, Kohl, and Paulsen [74].

**c. Comparison of our model vs Chen *et al.* [75]**

Figure 2 from Chen *et al.* [75] was evaluated. The mean duration of the active state in control cortical slabs was obtained from the text. The authors quoted a range for the duration of the active states in the cortical slabs with the application of bicuculline. A range of fold decrease in duration of active state with application of bicuculline was calculated, with the assumption that the durations of active states were normally distributed. This was compared against the fold decrease in up state duration derived from our model ( $\varepsilon = 0.3$  Hz,  $\zeta = 0.5$ ,  $\tau_{synapse} = 25$  ms, [glucose] = 0.02 M) within Regime C near the border with Regime D ( $\nu = 6.5$  Hz) to the lower end of Regime E ( $\nu = 13$  Hz).

**d. Comparison of our model vs Huo *et al.* [76]**

Figure 1 from Huo *et al.* [76] was evaluated. The mean duration of up states and the average number of action potentials per active up state were both obtained from the text. The mean duration of up states was normalized by the mean duration of up states in the control condition, and the average number of action potentials per active up state was also normalized by the average number of action potentials per active up state in the control condition. These were then compared with results from our model. The variable components of input frequencies were chosen within Regime C (from Fig. 7) to approximate the fold change in the average number of action potentials per active up state in Huo *et al.* [76] experimental condition. The model was run with  $\varepsilon = 0.3$  Hz,  $\zeta = 0.5$ ,  $\tau_{synapse} = 25$  ms, [glucose] = 0.02 M and  $\nu = 6.5$  Hz (equivalent to control) and  $\nu = 5$  Hz (equivalent to experimental condition). The firing frequencies and up state durations were normalized to their respective values for the equivalent control condition.

**e. Comparison of our model vs Cunningham *et al.* [77]**

Figure 1 from Cunningham *et al.* [77] was evaluated. The durations of the down-phase periods as a function of the glucose concentration were obtained from the text. The down state durations were normalized by the down state durations at 10 mM glucose.

We then obtained equivalent data from our model. We compared simulations with the following critical parameters kept constant:  $\nu = 7$  Hz,  $\varepsilon = 0.3$  Hz,  $\zeta = 0.5$ ,  $\tau_{synapse} = 25$  ms. Glucose concentration was set at 0.03M and 0.015M, and the down state durations for these two simulations were calculated. The down state durations were then normalized by the down state durations at a [glucose] of 0.03M. These results were then plotted against those obtained from Cunningham *et al.* [77].

**f. Comparison of our model vs Castano-Prat *et al.* [78]**

Figure 2 from Castano-Prat *et al.* [78] was evaluated. Data points for up duration (s) versus age of mouse (3xTg mutant mouse only) (Fig. 2F from Castano-Prat *et al.* [78]) and down duration (s) versus age of mouse (3xTg mutant only) (Fig. 2C from Castano-Prat *et al.* [78]) were measured using the measuring tool in Adobe Acrobat DC (Adobe, San Jose, California), and the depicted data points were measured with a precision of 0.01 inches. These values were then scaled by the measured distances between the labeled marks on the figure axes to obtain numerical values for up and down state durations. The up and down state durations were normalized by the up and down state durations of the young 3xTg mutant mice, respectively. Durations of up and down states for the cortical areas (prelimbic cortex, primary motor cortex, primary somatosensory cortex, and primary visual cortex) were pooled by Castano-Prat *et al.*

We then obtained equivalent data from our model. We compared simulations with the following critical parameters kept constant:  $\nu = 7$  Hz,  $\varepsilon = 0.3$  Hz,  $\zeta = 0.5$ ,  $\tau_{synapse} = 25$  ms, [glucose] = 0.02 M. The reaction rate parameter ( $k_{veg}$ ) value for the “vegetative” use of ATP was set at 0.2 and 0.5, and the up and down state durations for these two simulations

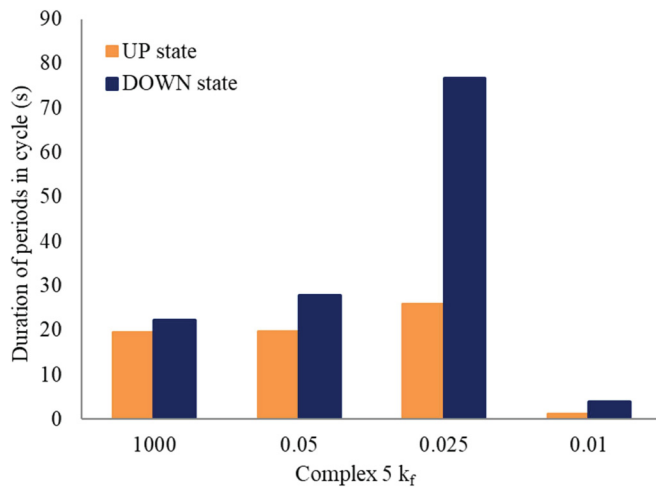


FIG. 17. Poisoning the mitochondrial electron transport chain process for energy generation alters the duration of up and down states.  $\varepsilon = 0.3$  Hz,  $\nu = 7$  Hz,  $\zeta = 0.5$ . The mitochondria supply the vast majority of ATP to all three components of the tripartite synapse. The complex 5  $k_f$  is the effective forward rate reaction constant for complex 5 generating ATP. As the  $k_f$  decreases, the efficiency of ATP generation decreases, and there is initially an increase in the durations of both the up state and the down state, although the increase in the down state is much more prominent than that in the up state. Eventually, when mitochondrial ATP generation is sufficiently impaired, the duration of the up and down states suddenly drops, indicating transition into Regime E with ATP limiting signal transmission in the tripartite synapse. The complex 5  $k_f$  was simultaneously varied in the presynaptic terminal, postsynaptic terminal, and astrocytic compartments, to replicate the presence of a mitochondrial toxin.

were calculated. The up and down state durations were then normalized by the up and down state durations at a  $k_{veg}$  of 0.2. These results were then plotted against those obtained from Castano-Prat *et al.* [78].

### 8. Predictions for a different experimental system

Our model allows for evaluation of mitochondrial dysfunction, and its effects on the functioning of the tripartite synapse. We evaluated the effects of decreasing the efficiency of the mitochondrial electron transport chain, specifically at mitochondrial complex 5, a procedure which simulates the introduction of a mitochondrial complex 5 toxin (Fig. 17). We found that, like with increasing vegetative ATP use, “poisoning” mitochondrial complex 5 initially led to increased durations for both the up and the down states, prior to a transition into Regime E. In combination with the results of the simulations with decreased glucose, and increased “vegetative” ATP use, this suggests that energy shortage, regardless of cause (decreased substrate causing decreased generation, increased use, or direct decreased generation) leads to manifestation of Regime E.

### 9. Analysis of experimental systems and rationale for hypotheses

Here we present our hypotheses generated by the results of our model, and analyze how the hypotheses are applied

to the experimental systems evaluated, in addition to other pathological conditions.

#### a. Hypothesis 1: Mechanisms leading to increased firing rate will lead to operation of the tripartite synapse in Regime E

The experimental systems by Skrempou; Mann, Kohl, and Paulsen; Chen *et al.*; and Huo *et al.* each exhibits changes in up and down state durations due to altered firing rates [73–76]. Skrempou’s work actually showed evolution of up state durations over time, similar to transitions in our model from Regime C to (Regime D to) Regime E with increasing variable component of input firing frequency ( $\nu$ ). The transitions in Skrempou’s model system were attributed to progressively increased excitability caused by a gradual release of NMDA receptor blockade [73]. Kovac *et al.* [102] has shown that the increased activity in a low-magnesium model is dependent on vesicular glutamate release and on activation of the NMDA receptor, supporting the concept of increased firing rate as the mechanism for excitation. They also observed that neuronal ATP appeared to be depleted in an activity-dependent fashion in their model. Interestingly, Shindo *et al.* [103] demonstrated that glutamatergic excitotoxicity leads to extrusion of magnesium from neurons, and inhibitors of that extrusion both attenuated cell death and attenuated the decrease in intracellular ATP caused by excitotoxicity. This suggests that a lack of ATP may also contribute to the transition into Regime E-like behavior seen in the low-magnesium model. The exact mechanism of ATP depletion in low-magnesium states is unclear, as magnesium plays important roles in numerous cellular reactions, both related to energy metabolism and otherwise [104]. Indeed, the role of magnesium is complex even in the functioning of a single enzyme complex, the mitochondrial ATP synthase [105].

Rather than increasing excitation, both Mann, Kohl, and Paulsen and Chen *et al.* [74,75] blocked inhibition by applying a GABA<sub>A</sub> receptor antagonist. This blockade of inhibition led to increasing firing frequencies and consequently significantly decreased up state durations. This corresponds with transitions from Regime C or Regime D into Regime E with increased  $\nu$  in our model. Thus, increasing input firing frequency, whether by increasing excitation (low-magnesium model) or by decreasing inhibition (inhibition of GABAergic neurotransmission), leads to operation of the tripartite synapse in Regime E.

Finally, although Huo *et al.* [76] concluded that knocking out APP led to hyperexcitability of neural network activity (due to prolonged up state durations), they actually demonstrated that this alteration led to *both* a prolongation of up state duration *and* a decrease in the firing frequency (average number of action potentials per active up state) of the neurons. This suggests that the network was actually becoming less excitable, and corresponds to moving along the curve toward the left (*lower*  $\nu$ ) in Fig. 7. The only regime in which the up duration changes and the down duration stays constant, as found by Huo *et al.* [76], is Regime C. While this model did not show a transition into Regime E, the behavior of the system with decreasing firing frequency is consistent with the results of our model.

**b. Hypothesis 2: Severely decreased flux through the TCA cycle will lead to operation of the tripartite synapse in Regime E**

Cunningham *et al.* found that the up state duration remained approximately constant while the down state duration increased, with decreasing glucose [77], in line with our findings. However, they did not investigate the durations of the up and down states with even lower glucose concentrations; we are not aware of any groups that have directly examined up and down states in severely hypoglycemic neurons to test hypothesis (2). However, it is well known that severe hypoglycemia can lead to seizures [106], and it may be that the seizure-like activity is related to a similar transition into a Regime E-like firing pattern *in vivo*, caused by insufficient ATP. Intriguingly, focal seizures can also be seen in another condition, hyperosmolar hyperglycemic state (HHS; also called nonketotic hyperglycemia). Various possible mechanisms have been suggested for this, including metabolic derangements (hyperosmolarity, dehydration, or hyponatremia), increased metabolism of GABA for energy, inhibition of the Krebs (TCA) cycle, and focal cerebral ischemia [107–109]. Increased metabolism of GABA, the major inhibitory neurotransmitter in the brain, would lead to increased firing rate, resulting in a Regime E-like firing pattern. Inhibition of the TCA cycle and focal cerebral ischemia both suggest the absence of adequate energy stores, again leading to a Regime E-like firing pattern. It has also been noted that the focal seizures may be reflex seizures (seizures caused by sensory input), posture-induced seizures (seizures caused by “active or passive movement or posturing of a body part” [109]), or occipital lobe seizures (involving the visual cortex, the part of the brain that processes vision) [107]. Metabolic abnormalities typically induce *generalized* seizures [107]. We speculate that focal seizures occur in HHS when those *focal* areas tip over into Regime E from additional, use-dependent, neuronal activity (from processing sensory information or performing motor actions).

**c. Hypothesis 3: Increased non-neurotransmission-related use of ATP will lead to operation of the tripartite synapse in Regime E**

As described previously, proteinopathies such as Alzheimer’s disease represent good models for increased non-neurotransmission-related use of ATP. Castano-Prat

*et al.* found that elderly mice with increased brain pathology had longer durations of down states (and a trend toward longer duration in up states) [78]. We modeled the increased pathological protein load as an increase in the “vegetative” use of neuronal ATP, and found that initially both up and down state durations increased with increasing “vegetative” ATP use, as in the experimental model. However, when this “vegetative” ATP use was increased further, the up and down state durations significantly decreased, with the model transitioning into Regime E. We are not aware of any experiments evaluating up and down state durations in even more severe models of proteinopathy, to test hypothesis (3). However, it has been found that both “network hyperexcitability” and seizures can occur during even the early stages of Alzheimer’s disease [110]. In multiple sclerosis, a neuroinflammatory disorder with later neurodegenerative features, it is known that neuronal-glia metabolic interactions are disrupted, and it has been noted that there is increased synaptic transmission of pain signals, as well as a loss of interneurons [111]. Seizures also occur in multiple sclerosis, and it has been speculated that this may be due in part to loss of GABAergic neurons, or possibly due to dysregulated glutamate processing by astrocytes [112]. We wonder whether seizures occur in multiple sclerosis due to a loss of sufficient energy resources from the combination of disruption of normal neuronal-glia metabolic processes, increased non-neurotransmission-related energy expenditure, and loss of inhibitory interneurons (leading to increased firing rate), and it would be interesting to evaluate the changes in up and down state durations that may occur in this pathology.

**d. Hypothesis 4: Mitochondrial toxins will lead to operation of the tripartite synapse in Regime E**

Regarding hypothesis (4), we are not aware of any investigation into the duration of up and down states in mitochondrial dysfunction, either genetic or due to toxins, although there has recently been the development of a model of mitochondrial epilepsy which could investigate this scenario [113]. Of note, however, in living systems, mitochondrial dysfunction may lead to premature cell death prior to the development of Regime E. We hope that the hypotheses generated through analysis of our model will spur further experimental exploration using this and other systems.

- 
- [1] D. Jercog, A. Roxin, P. Bartho, A. Luczak, A. Compte, and J. de la Rocha, Up-down cortical dynamics reflect state transitions in a bistable network, *eLife* **6**, e22425 (2017).
- [2] M. Steriade, A. Nunez, and F. Amzica, A novel slow (< 1 Hz) oscillation of neocortical neurons in vivo: Depolarizing and hyperpolarizing components, *J. Neurosci.* **13**, 3252 (1993).
- [3] V. V. Vyazovskiy, U. Olcese, E. C. Hanlon, Y. Nir, C. Cirelli, and G. Tononi, Local sleep in awake rats, *Nature (London)* **472**, 443 (2011).
- [4] V. V. Vyazovskiy and K. D. Harris, Sleep and the single neuron: The role of global slow oscillations in individual cell rest, *Nat. Rev. Neurosci.* **14**, 443 (2013).
- [5] A. Destexhe, S. W. Hugers, M. Rudolph, and V. Crunelli, Are corticothalamic up states fragments of wakefulness? *Trends Neurosci.* **30**, 334 (2007).
- [6] D. Holcman and M. Tsodyks, The emergence of Up and Down states in cortical networks, *PLoS Comput. Biol.* **2**, e23 (2006).
- [7] B. L. Lewis and P. O’Donnell, Ventral tegmental area afferents to the prefrontal cortex maintain membrane potential ‘up’ states in pyramidal neurons via D<sub>1</sub> dopamine receptors, *Cereb. Cortex* **10**, 1168 (2000).
- [8] E. M. Tartaglia and N. Brunel, Bistability and up/down state alternations in inhibition-dominated randomly connected networks of LIF neurons, *Sci. Rep.* **7**, 11916 (2017).

- [9] S. Scarpetta and A. de Candia, Alternation of up and down states at a dynamical phase-transition of a neural network with spatiotemporal attractors, *Front. Syst. Neurosci.* **8**, 88 (2014).
- [10] J. D. Cowan, J. Neuman, and W. van Drongelen, Wilson-Cowan equations for neocortical dynamics, *J. Math. Neurosci.* **6**, 1 (2016).
- [11] H. R. Wilson and J. D. Cowan, Excitatory and inhibitory interactions in localized populations of model neurons, *Biophys. J.* **12**, 1 (1972).
- [12] R. Brette, What is the most realistic single-compartment model of spike initiation? *PLoS Comput. Biol.* **11**, e1004114 (2015).
- [13] R. Jolivet, A. Rauch, H. Lüscher, and W. Gerstner, Predicting spike timing of neocortical pyramidal neurons by simple threshold models, *J. Comput. Neurosci.* **21**, 35 (2006).
- [14] N. Parga and L. F. Abbott, Network model of spontaneous activity exhibiting synchronous transitions between up and down states, *Front. Neurosci.* **1**, 57 (2007).
- [15] H. Setareh, M. Deger, C. C. H. Petersen, and W. Gerstner, Cortical dynamics in presence of assemblies of densely connected weight-hub neurons, *Front. Comput. Neurosci.* **11**, 52 (2017).
- [16] I. Timofeev, F. Grenier, M. Bazhenov, T. J. Sejnowski, and M. Steriade, Origin of slow cortical oscillations in deafferented cortical slabs, *Cereb. Cortex* **10**, 1185 (2000).
- [17] M. Bazhenov, I. Timofeev, M. Steriade, and T. J. Sejnowski, Model of thalamocortical slow-wave sleep oscillations and transitions to activated states, *J. Neurosci.* **22**, 8691 (2002).
- [18] S. Hill and G. Tononi, Modeling sleep and wakefulness in the thalamocortical system, *J. Neurophysiol.* **93**, 1671 (2005).
- [19] A. L. Hodgkin and A. F. Huxley, A quantitative description of membrane current and its application to conduction and excitation in nerve, *J. Physiol.* **117**, 500 (1952).
- [20] A. L. Hodgkin, A. F. Huxley, and B. Katz, Measurement of current-voltage relations in the membrane of the giant axon of *Loligo*, *J. Physiol.* **116**, 424 (1952).
- [21] S. Ching, P. L. Purdon, S. Vijayan, N. J. Kopell, and E. N. Brown, A neurophysiological-metabolic model for burst suppression, *Proc. Nat. Acad. Sci. USA* **109**, 3095 (2012).
- [22] C. Cakan and K. Obermayer, Biophysically grounded mean-field models of neural populations under electrical stimulation, *PLoS Comput. Biol.* **16**, e1007822 (2020).
- [23] E. Ledoux and N. Brunel, Dynamics of networks of excitatory and inhibitory neurons in response to time-dependent inputs, *Front. Comput. Neurosci.* **5**, 25 (2011).
- [24] E. Negahbani, D. A. Steyn-Ross, M. L. Steyn-Ross, M. T. Wilson, and J. W. Sleight, Noise-induced precursors of state transitions in the stochastic Wilson-Cowan model, *J. Math. Neurosci.* **5**, 9 (2015).
- [25] A. Destexhe and T. J. Sejnowski, The Wilson-Cowan model, 36 years later, *Biol. Cybern.* **101**, 1 (2009).
- [26] C. T. Li, M. Poo, and Y. Dan, Burst spiking of a single cortical neuron modifies global brain state, *Science* **324**, 643 (2009).
- [27] S. Fujisawa, N. Matsuki, and Y. Ikegaya, Single neurons can induce phase transitions of cortical recurrent networks with multiple internal states, *Cereb. Cortex* **16**, 639 (2006).
- [28] S. P. Muscinelli, W. Gerstner, and T. Schwalger, How single neuron properties shape chaotic dynamics and signal transmission in random neural networks, *PLoS Comput. Biol.* **15**, e1007122 (2019).
- [29] F. Oschmann, H. Berry, K. Obermayer, and K. Lenk, From in silico astrocyte cell models to neuron-astrocyte network models: A review, *Brain Res. Bull.* **136**, 76 (2018).
- [30] L. Øyehaug, I. Østby, C. M. Lloyd, S. W. Omholt, and G. T. Einevoll, Dependence of spontaneous neuronal firing and depolarisation block on astroglial membrane transport mechanisms, *J. Comput. Neurosci.* **32**, 147 (2012).
- [31] D. E. Postnov, L. S. Ryazanova, N. A. Brazhe, A. R. Brazhe, G. V. Maximov, E. Mosekilde, and O. V. Sosnovtseva, Giant glial cell: New insight through mechanism-based modeling, *J. Biol. Phys.* **34**, 441 (2008).
- [32] S. Nadkarni and P. Jung, Spontaneous Oscillations of Dressed Neurons: A New Mechanism for Epilepsy? *Phys. Rev. Lett.* **91**, 268101 (2003).
- [33] J. S. Diamond, Deriving the glutamate clearance time course from transporter currents in CA1 hippocampal astrocytes: Transmitter uptake gets faster during development, *J. Neurosci.* **25**, 2906 (2005).
- [34] D. A. Rusakov, The role of perisynaptic glial sheaths in glutamate spillover and extracellular  $\text{Ca}^{2+}$  depletion, *Biophys. J.* **81**, 1947 (2001).
- [35] M. De Pittà and N. Brunel, Modulation of synaptic plasticity by glutamatergic gliotransmission: A modeling study, *Neural Plast.* **2016**, 7607924 (2016).
- [36] S. G. Tewari and K. K. Majumdar, A mathematical model of the tripartite synapse: Astrocyte-induced synaptic plasticity, *J. Biol. Phys.* **38**, 465 (2012).
- [37] J. J. Wade, L. J. McDaid, J. Harkin, V. Crunelli, and J. A. S. Kelso, Bidirectional coupling between astrocytes and neurons mediates learning and dynamic coordination in the brain: A multiple modeling approach, *PLoS ONE* **6**, e29445 (2011).
- [38] R. Jolivet, J. S. Coggan, I. Allaman, and P. J. Magistretti, Multi-timescale modeling of activity-dependent metabolic coupling in the neuron-glia-vasculature ensemble, *PLoS Comput. Biol.* **11**, e1004036 (2015).
- [39] A. B. Patel, R. A. de Graaf, G. F. Mason, T. Kanamatsu, D. L. Rothman, R. G. Shulman, and K. L. Behar, Glutamatergic neurotransmission and neuronal glucose oxidation are coupled during intense neuronal activation, *J. Cereb. Blood Flow Metab.* **24**, 972 (2004).
- [40] R. Occhipinti, E. Somersalo, and D. Calvetti, Astrocytes as the glucose shunt for glutamatergic neurons at high activity: An in silico study, *J. Neurophysiol.* **101**, 2528 (2009).
- [41] R. Occhipinti, E. Somersalo, and D. Calvetti, Energetics of inhibition: Insights with a computational model of the human GABAergic neuron-astrocyte cellular complex, *J. Cereb. Blood Flow Metab.* **30**, 1834 (2010).
- [42] D. Calvetti and E. Somersalo, Ménage à trois: The role of neurotransmitters in the energy metabolism of astrocytes, glutamatergic, and GABAergic neurons, *J. Cereb. Blood Flow Metab.* **32**, 1472 (2012).
- [43] T. Cakir, S. Alsan, H. Saybaşili, A. Akin, and K. O. Ülgen, Reconstruction and flux analysis of coupling between metabolic pathways of astrocytes and neurons: Application to cerebral hypoxia, *Theor. Biol. Med. Model.* **4**, 48 (2007).
- [44] M. C. McKenna, The glutamate-glutamine cycle is not stoichiometric: Fates of glutamate in brain, *J. Neurosci. Res.* **85**, 3347 (2007).
- [45] J. Shen, K. F. Petersen, K. L. Behar, P. Brown, T. W. Nixon, G. F. Mason, O. A. Petroff, G. I. Shulman, R. G. Shulman,

- and D. L. Rothman, Determination of the rate of the glutamate/glutamine cycle in the human brain by *in vivo*  $^{13}\text{C}$  NMR, *Proc. Nat. Acad. Sci. USA* **96**, 8235 (1999).
- [46] See Supplemental Material at <http://link.aps.org/supplemental/10.1103/PhysRevE.107.024415> for specification of model, equations, tables of parameters, example initial conditions, rules, and events.
- [47] J. M. Berg, J. L. Tymoczko, and L. Stryer, *Biochemistry*, 6th ed. (W. H. Freeman, New York, 2007).
- [48] E. Engl and D. Attwell, Non-signalling energy use in the brain, *J. Physiol.* **593**, 3417 (2015).
- [49] D. Pathak, L. Y. Shields, B. A. Mendelsohn, D. Haddad, W. Lin, A. A. Gerencser, H. Kim, M. D. Brand, R. H. Edwards, and K. Nakamura, The role of mitochondrially derived ATP in synaptic vesicle recycling, *J. Biol. Chem.* **290**, 22325 (2015).
- [50] D. Purves, G. J. Augustine, D. Fitzpatrick, W. C. Hall, A.-S. LaMantia, J. O. McNamara, and L. E. White, *Neuroscience*, 4th ed. (Sinauer Associates, Sunderland, MA, 2008).
- [51] J. C. Fiala and K. M. Harris, Dendrite structure, in *Dendrites*, edited by G. Stuart, M. Häusser, and N. Spruston (Oxford University Press, New York, 1999), pp. 1–34.
- [52] D. Attwell and S. B. Laughlin, An energy budget for signaling in the grey matter of the brain, *J. Cereb. Blood Flow Metab.* **21**, 1133 (2001).
- [53] N. J. Gerkau, R. Lerchundi, J. S. E. Nelson, M. Lantermann, J. Meyer, J. Hirrlinger, and C. R. Rose, Relationship between activity-induced intracellular sodium transients and ATP dynamics in mouse hippocampal neurons, *J. Physiol.* **597**, 5687 (2019).
- [54] K. Ikeda and J. M. Bekkers, Counting the number of releasable synaptic vesicles in a presynaptic terminal, *Proc. Nat. Acad. Sci. USA* **106**, 2945 (2009).
- [55] L. Pellerin and P. J. Magistretti, Sweet sixteen for ANLS, *J. Cereb. Blood Flow Metab.* **32**, 1152 (2012).
- [56] A. Schousboe, H. S. Waagepetersen, and U. Sonnewald, Astrocytic pyruvate carboxylation: Status after 35 years, *J. Neurosci. Res.* **97**, 890 (2019).
- [57] G. Yellen, Fueling thought: Management of glycolysis and oxidative phosphorylation in neuronal metabolism, *J. Cell Biol.* **217**, 2235 (2018).
- [58] A. Falkowska, I. Gutowska, M. Goschorska, P. Nowacki, D. Chlubek, and I. Baranowska-Bosiacka, Energy metabolism of the brain, including the cooperation between astrocytes and neurons, especially in the context of glycogen metabolism, *Int. J. Mol. Sci.* **16**, 25959 (2015).
- [59] I. M. Raman and L. O. Trussell, The mechanism of alpha-amino-3-hydroxy-5-methyl-4-isoxazolepropionate receptor desensitization after removal of glutamate, *Biophys. J.* **68**, 137 (1995).
- [60] F. A. Chaudhry, D. Schmitz, R. J. Reimer, P. Larsson, A. T. Gray, R. Nicoll, M. Kavanaugh, and R. H. Edwards, Glutamine uptake by neurons: Interaction of protons with system A transporters, *J. Neurosci.* **22**, 62 (2002).
- [61] Y. Wang, Y. Li, R. Zhao, B. Wu, B. Lanoha, Z. Tong, J. Peer, J. Liu, H. Xiong, Y. Huang, and J. Zheng, Glutaminase C overexpression in the brain induces learning deficits, synaptic dysfunctions, and neuroinflammation in mice, *Brain Behav. Immun.* **66**, 135 (2017).
- [62] M. Martineau, R. E. Guzman, C. Fahlke, and J. Klingauf, VG-LUT1 functions as a glutamate/proton exchanger with chloride channel activity in hippocampal glutamatergic synapses, *Nat. Commun.* **8**, 2279 (2017).
- [63] B. Zhang, Q. Jin, L. Xu, N. Li, Y. Meng, S. Chang, X. Zheng, J. Wang, Y. Chen, D. Neculai *et al.*, Cooperative transport mechanism of human monocarboxylate transporter 2, *Nat. Commun.* **11**, 2429 (2020).
- [64] A. P. Halestrap, The monocarboxylate transporter family—Structure and functional characterization, *IUBMB Life* **64**, 1 (2012).
- [65] E. A. Angamo, J. Rösner, A. Liotta, R. Kovács, and U. Heinemann, A neuronal lactate uptake inhibitor slows recovery of extracellular ion concentration changes in the hippocampal CA3 region by affecting energy metabolism, *J. Neurophysiol.* **116**, 2420 (2016).
- [66] H. Koepsell, Glucose transporters in brain in health and disease, *Pflügers Arch.* **472**, 1299 (2020).
- [67] M. B. Robinson and J. G. Jackson, Astroglial glutamate transporters coordinate excitatory signaling and brain energetics, *Neurochem. Int.* **98**, 56 (2016).
- [68] L. Pochini, M. Scalise, M. Galluccio, and C. Indiveri, Membrane transporters for the special amino acid glutamine: Structure/function relationships and relevance to human health, *Front. Chem.* **2**, 61 (2014).
- [69] A. Bröer, N. Brookes, V. Ganapathy, K. S. Dimmer, C. A. Wagner, F. Lang, and S. Bröer, The astroglial ASCT2 amino acid transporter as a mediator of glutamine efflux, *J. Neurochem.* **73**, 2184 (1999).
- [70] A. Plaitakis, E. Kalef-Ezra, D. Kotzamani, I. Zaganas, and C. Spanaki, The glutamate dehydrogenase pathway and its roles in cell and tissue biology in health and disease, *Biology (Basel)* **6**, 11 (2017).
- [71] N. Nguyen, S. V. Gonzalez, and B. Hassel, Formation of glycerol from glucose in rat brain and cultured brain cells. Augmentation with kainate or ischemia, *J. Neurochem.* **101**, 1694 (2007).
- [72] D. M. Ramirez and E. T. Kavalali, Differential regulation of spontaneous and evoked neurotransmitter release at central synapses, *Curr. Opin. Neurobiol.* **21**, 275 (2011).
- [73] G. Skrepmpou, *Who gives in first? Region-specific vulnerability to epileptogenesis and the role of the endogenous cortical network activity* (Department of Biology, National and Kapodistrian University of Athens, Athens, Greece, 2020).
- [74] E. O. Mann, M. M. Kohl, and O. Paulsen, Distinct roles of GABA(A) and GABA(B) receptors in balancing and terminating persistent cortical activity, *J. Neurosci.* **29**, 7513 (2009).
- [75] J. Y. Chen, S. Chauvette, S. Skorheim, I. Timofeev, and M. Bazhenov, Interneuron-mediated inhibition synchronizes neuronal activity during slow oscillation, *J. Physiol.* **590**, 3987 (2012).
- [76] Q. Huo, M. Chen, Q. He, J. Zhang, B. Li, K. Jin, X. Chen, C. Long, and L. Yang, Prefrontal cortical GABAergic dysfunction contributes to aberrant up-state duration in APP knockout mice, *Cereb. Cortex* **27**, 4060 (2017).
- [77] M. Cunningham, D. Pervouchine, C. Racca, N. Kopell, C. Davies, R. Jones, R. Traub, and M. Whittington, Neuronal metabolism governs cortical network response state, *Proc. Nat. Acad. Sci. USA* **103**, 5597 (2006).
- [78] P. Castano-Prat, L. Perez-Mendez, M. Perez-Zabalza, C. Sanfeliu, L. Gimenez-Llort, and M. Sanchez-Vives, Altered slow (<1 Hz) and fast (beta and gamma) neocortical

- oscillations in the 3xTg-AD mouse model of Alzheimer's diseases under anesthesia, *Neurobiol. Aging* **79**, 142 (2019).
- [79] G. Buzsáki, C. A. Anastassiou, and C. Koch, The origin of extracellular fields and currents—EEG, ECoG, LFP, and spikes, *Nat. Rev. Neurosci.* **13**, 407 (2012).
- [80] A. B. Patel, R. A. de Graaf, G. F. Mason, D. L. Rothman, R. G. Shulman, and K. L. Behar, The contribution of GABA to glutamate/glutamine cycling and energy metabolism in the rat cortex in vivo, *Proc. Nat. Acad. Sci. USA* **102**, 5588 (2005).
- [81] Y. Yu, P. Herman, D. L. Rothman, D. Agarwal, and F. Hyder, Evaluating the gray and white matter energy budgets of human brain function, *J. Cereb. Blood Flow Metab.* **38**, 1339 (2018).
- [82] P. J. Magistretti, Neuron-glia metabolic coupling and plasticity, *J. Exp. Biol.* **209**, 2304 (2006).
- [83] M. Belanger, I. Allaman, and P. J. Magistretti, Brain energy metabolism: Focus on astrocyte-neuron metabolic cooperation, *Cell Metab.* **14**, 724 (2011).
- [84] M. V. Sanchez-Vives and M. Mattia, Slow wave activity as the default mode of the cerebral cortex, *Arch. Ital. Biol.* **152**, 147 (2014).
- [85] R. S. Zucker and W. G. Regehr, Short-term synaptic plasticity, *Annu. Rev. Physiol.* **64**, 355 (2002).
- [86] R. Rosenbaum, J. Rubin, and B. Doiron, Short term synaptic depression imposes a frequency dependent filter on synaptic information transfer, *PLoS Comput. Biol.* **8**, e1002557 (2012).
- [87] F. Siclari and G. Tononi, Local aspects of sleep and wakefulness, *Curr. Opin. Neurobiol.* **44**, 222 (2017).
- [88] J. M. Krueger, J. T. Nguyen, C. J. Dykstra-Aiello, and P. Taishi, Local sleep, *Sleep Med. Rev.* **43**, 14 (2019).
- [89] R. Huber, M. F. Ghilardi, M. Massimini, F. Ferrarelli, B. A. Riedner, M. J. Peterson, and G. Tononi, Arm immobilization causes cortical plastic changes and locally decreases sleep slow wave activity, *Nat. Neurosci.* **9**, 1169 (2006).
- [90] A. Quercia, F. Zappasodi, G. Committeri, and M. Ferrara, Local use-dependent sleep in wakefulness links performance errors to learning, *Front. Hum. Neurosci.* **12**, 122 (2018).
- [91] H. Kattler, D. J. Dijk, and A. A. Borbely, Effect of unilateral somatosensory stimulation prior to sleep on the sleep EEG in humans, *J. Sleep Res.* **3**, 159 (1994).
- [92] Y. Nir, R. J. Staba, T. Andrillon, V. V. Vyazovskiy, C. Cirelli, I. Fried, and G. Tononi, Regional slow waves and spindles in human sleep, *Neuron* **70**, 153 (2011).
- [93] A. Silvani, V. Asti, C. Berteotti, V. Ferrari, C. Franzini, P. Lenzi, J. Wild, D. A. Grant, A. M. Walker, and G. Zoccoli, Sleep-dependent changes in cerebral oxygen consumption in newborn lambs, *J. Sleep Res.* **15**, 206 (2006).
- [94] J. Schneider, N. Berndt, I. E. Papageorgiou, J. Maurer, S. Bulik, M. Both, A. Draguhn, H. Holzhütter, and O. Kann, Local oxygen homeostasis during various neuronal network activity states in the mouse hippocampus, *J. Cereb. Blood Flow Metab.* **39**, 859 (2019).
- [95] J. M. Krueger, M. G. Frank, J. P. Wisor, and S. Roy, Sleep function: Toward elucidating an enigma, *Sleep Med. Rev.* **28**, 46 (2016).
- [96] U. S. Bhalla and J. M. Bower, Exploring parameter space in detailed single neuron models: Simulations of the mitral and granule cells of the olfactory bulb, *J. Neurophysiol.* **69**, 1948 (1993).
- [97] K. Gadhve, N. Bolshette, A. Ahire, R. Pardeshi, K. Thakur, C. Trandafir, A. Istrate, S. Ahmed, M. Lahkar, D. Muresanu, and M. Balea, The ubiquitin proteasomal system: A potential target for the management of Alzheimer's disease, *J. Cell. Mol. Med.* **20**, 1392 (2016).
- [98] J. Bard, E. Goodall, E. Greene, E. Jonsson, K. Dong, and A. Martin, Structure and function of the 26S proteasome, *Annu. Rev. Biochem.* **87**, 697 (2018).
- [99] R. Singh and A. Cuervo, Autophagy in the cellular energetic balance, *Cell Metab.* **13**, 495 (2011).
- [100] R. Lackie, A. Maciejewski, V. Ostapchenko, J. Marques-Lopez, W.-Y. Choy, M. Duennwald, V. Prado, and M. Prado, The Hsp70/Hsp90 chaperone machinery in neurodegenerative diseases, *Front. Neurosci.* **11**, 254 (2017).
- [101] B. Boland, W. Yu, O. Corti, B. Mollereau, A. Henriques, E. Bezard, G. Pastores, D. Rubinsztein, R. Nixon, M. Duchet *et al.*, Promoting the clearance of neurotoxic proteins in neurodegenerative disorders of ageing, *Nat. Rev. Drug Discov.* **17**, 660 (2018).
- [102] S. Kovac, A. Domijan, M. C. Walker, and A. Y. Abramov, Prolonged seizure activity impairs mitochondrial bioenergetics and induces cell death, *J. Cell Sci.* **125**, 1796 (2012).
- [103] Y. Shindo, R. Yamanaka, K. Hotta, and K. Oka, Inhibition of Mg<sup>2+</sup> extrusion attenuates glutamate excitotoxicity in cultured rat hippocampal neurons, *Nutrients* **12**, 2768 (2020).
- [104] I. Pilchova, K. Klacanova, Z. Tatkova, P. Kaplan, and P. Racay, The involvement of Mg<sup>2+</sup> in regulation of cellular and mitochondrial functions, *Oxid. Med. Cell. Longev.* **2017**, 6797460 (2017).
- [105] P. D. Boyer, Catalytic site forms and controls in ATP synthase catalysis, *Biochim. Biophys. Acta* **1458**, 252 (2000).
- [106] M. Maheandiran, S. Mylvaganam, C. Wu, Y. El-Hayek, S. Sugumar, L. Hazrati, M. del Campo, A. Giacca, L. Zhang, and P. Carlen, Severe hypoglycemia in a juvenile diabetic rat model: Presence and severity of seizures are associated with mortality, *PLoS ONE* **8**, e83168 (2013).
- [107] U. K. Misra, J. Kalita, S. K. Bhoi, and D. Dubey, Spectrum of hyperosmolar hyperglycaemic state in neurology practice, *Indian J. Med. Res.* **146**, S1 (2017).
- [108] X. Wang, H. Yu, Z. Cai, Z. Wang, B. Ma, and Y. Zhang, Nonketotic hyperglycemia-related epileptic seizures, *Epilepsy Behav. Case Rep.* **1**, 77 (2013).
- [109] J. F. Brick, J. A. Gutrecht, and R. A. Ringel, Reflex epilepsy and nonketotic hyperglycemia in the elderly: A specific neuroendocrine syndrome, *Neurology* **39**, 394 (1989).
- [110] K. A. Vossel, M. C. Tartaglia, H. B. Nygaard, A. Z. Zeman, and B. L. Miller, Epileptic activity in Alzheimer's disease: Causes and clinical relevance, *Lancet Neurol.* **16**, 311 (2017).
- [111] R. R. Robinson, A. K. Dietz, A. M. Maroof, R. Asmis, and T. G. Forsthuber, The role of glial-neuronal metabolic cooperation in modulating progression of multiple sclerosis and neuropathic pain, *Immunotherapy* **11**, 129 (2019).

- [112] A. S. Lapato, S. M. Thompson, K. Parra, and S. K. Tiwari-Woodruff, Astrocyte glutamate uptake and water homeostasis are dysregulated in the hippocampus of multiple sclerosis patients with seizures, *ASN Neuro* **12**, 1759091420979604 (2020).
- [113] F. Chan, N. Z. Lax, C. M. Voss, B. I. Aldana, S. Whyte, A. Jenkins, C. Nicholson, S. Nichols, E. Tilley, Z. Powell *et al.*, The role of astrocytes in seizure generation: Insights from a novel *in vitro* seizure model based on mitochondrial dysfunction, *Brain* **142**, 391 (2019).